

Water Resources Research

RESEARCH ARTICLE

10.1029/2024WR037606

Key Points:

- Groundwater age distributions indicate somewhat continuous recharge from Last Glacial Maximum to present in semi-arid alluvial basin
- Isotopic and noble gas tracers reveal maximum water table depths and reduction in wintertime precipitation during Mid-Holocene arid period
- Natural fluctuations in groundwater recharge have been small compared to pumping-induced declines in regional water table

Supporting Information:

Supporting Information may be found in the online version of this article.

Correspondence to:

J. C. McIntosh,
jennmc@arizona.edu

Citation:

Noyes, C., Ferguson, G., Seltzer, A., Ng, J., Carroll, K. C., Tyne, R., et al. (2025). Variations in groundwater recharge and water table elevations across the Holocene in a semi-arid alluvial basin. *Water Resources Research*, 61, e2024WR037606. <https://doi.org/10.1029/2024WR037606>

Received 25 MAR 2024

Accepted 23 JUL 2025

Author Contributions:

Conceptualization: Chandler Noyes, Jennifer C. McIntosh

Formal analysis: Chandler Noyes, Alan Seltzer, Jessica Ng, Katherine Markovich, Roland Purtschert, Jeffrey Severinghaus

Funding acquisition: Chandler Noyes, Martin Stute

Investigation: Kenneth C. Carroll









Methodology: Chandler Noyes, Alan Seltzer, Jessica Ng, Roland Purtschert, Martin Stute, Jeffrey Severinghaus

Supervision: Grant Ferguson, Jennifer C. McIntosh

© 2025 The Author(s).

This is an open access article under the terms of the [Creative Commons Attribution-NonCommercial License](https://creativecommons.org/licenses/by-nc/4.0/), which permits use, distribution and reproduction in any medium, provided the original work is properly cited and is not used for commercial purposes.

Variations in Groundwater Recharge and Water Table Elevations Across the Holocene in a Semi-Arid Alluvial Basin

Chandler Noyes^{1,2}, Grant Ferguson^{1,3} , Alan Seltzer⁴ , Jessica Ng⁵ , Kenneth C. Carroll⁶ , Rebecca Tyne⁴ , Katherine Markovich^{7,8}, Roland Purtschert⁹, Martin Stute¹⁰ , Jeffrey Severinghaus⁵ , and Jennifer C. McIntosh^{1,3} 

¹Hydrology and Atmospheric Sciences, University of Arizona, Tucson, AZ, USA, ²Waite-Heindel Environmental Management, Burlington, VT, USA, ³Civil, Geological, and Environmental Engineering, University of Saskatchewan, Saskatoon, SK, Canada, ⁴Woods Hole Oceanographic Institution, Woods Hole, MA, USA, ⁵Scripps Institution of Oceanography, University of California San Diego, La Jolla, CA, USA, ⁶Plant and Environmental Sciences, New Mexico State University, Las Cruces, NM, USA, ⁷INTERA Incorporated, Albuquerque, NM, USA, ⁸Now with United States Geological Survey Upper Midwest Water Science Center, Mounds View, MN, USA, ⁹Climate and Environmental Physics, University of Bern, Bern, Switzerland, ¹⁰Lamont-Doherty Earth Observatory, Columbia University, Palisades, NY, USA

Abstract Many regional aquifer systems undergoing depletion contain “fossil” groundwater recharged under different climate conditions, raising questions on groundwater renewability. We examine the spatial distribution in groundwater ages estimated with multiple tracers covering different timescales, along with differences in paleoclimate and water table depths (WTD) in the Tucson Basin, Arizona, USA, to constrain recharge history. The presence of ³H and ⁸⁵Kr in upgradient wells indicates modern recharge, while ³⁹Ar, ¹⁴C, and ⁴He values show components of water several hundred to tens of thousands of years old in downgradient wells. In some wells, apparent ages on the orders of decades, centuries, and millennia are simultaneously indicated by ⁸⁵Kr, ³⁹Ar, and ¹⁴C activities, indicating that the flow system cannot be explained by a simple piston-flow model. To disentangle mixing and recharge history signals, we apply an inverse modeling technique that couples lumped parameter modeling of residence times with (stable) noble gas reconstructions of recharge temperature and WTD. A mid-Holocene maximum in WTD, reconstructed from Kr and Xe isotopes, suggests enhanced aridity associated with a reduction of wintertime precipitation, inferred from a shift in $\delta^{18}\text{O}$ and δD . Colder temperatures were present during the Last Glacial Maximum, reflecting both climatic cooling and cold mountain front recharge. Recharge to the Tucson Basin has been continuous since the LGM, albeit with a likely reduction during the mid-Holocene. Natural fluctuations in groundwater recharge have been small compared to those associated with groundwater extraction, indicating that pumping poses a larger threat to groundwater resources than climate change.

1. Introduction

Many regional aquifer systems undergoing depletion contain “fossil” groundwater, defined as water over 12,000 years old (Bierkens & Wada, 2019; Jasechko et al., 2017). Fossil groundwater is often thought to be non-renewable, because recharge is insufficient to replenish the aquifer on human timescales under background conditions (Bethke & Johnson, 2008; Bierkens & Wada, 2019; Margat et al., 2006). This approach can be misleading because groundwater age is a function of flow system size and position, neither of which are strongly related to how much depletion occurs during groundwater extraction (Ferguson et al., 2020). The link between groundwater age and renewability is further complicated by changes in groundwater flow systems once pumped that can create new sources of recharge through capture of streamflow (Bredehoeft, 2002; Konikow & Leake, 2014). Renewability of groundwater resources should not be defined in terms of groundwater recharge rates or groundwater age distributions but rather in terms of how the groundwater system responds to pumping (Cuthbert et al., 2023). However, if baseflow has been captured, groundwater recharge rates can be important in maintaining water levels in water supply wells (Butler et al., 2023). In such cases, understanding recharge rates over long time periods will provide some insights to developing groundwater resources in a manner that prevents further depletion.

Numerous studies globally have indicated that terrestrial climate was generally cooler during the end of the Last Ice Age, with pronounced regional differences in hydroclimate relative to the present (e.g., Liu et al., 2018; Tierney et al., 2020; Seltzer, Ng, et al., 2021). In particular, the U.S. Southwest was 5–7°C cooler during the late

Validation: Rebecca Tyne
Visualization: Chandler Noyes,
Grant Ferguson, Alan Seltzer
Writing – original draft: Chandler Noyes
Writing – review & editing:
Grant Ferguson, Alan Seltzer, Kenneth
C. Carroll, Rebecca Tyne,
Katherine Markovich, Roland Purtschert,
Jennifer C. McIntosh

Pleistocene (Kaufman et al., 2020; Phillips et al., 1986; Seltzer, Ng, et al., 2021; Zhu et al., 1998) with higher recharge rates (Manning, 2011; Phillips et al., 1986; Spaulding et al., 1983; Van Devender & Spaulding, 1979; Zhu et al., 1998). Considerably less is known about paleoclimate and groundwater recharge during the mid- to late-Holocene when there were prolonged periods of drought (Scanlon et al., 2006).

In semi-arid to arid regions where the water table is deep, an inherent temporal decoupling between groundwater flow and climate conditions may exist (Cuthbert et al., 2019), such that hydraulic response times are long, and aquifers may still be responding to shifts in climate that occurred thousands to hundreds of thousands of years ago (Cuthbert et al., 2019; Rousseau-Gueutin et al., 2013). For example, some aquifer systems containing fossil groundwater with negligible recharge today exhibit larger-than-expected hydraulic gradients with greater amounts of discharge than recharge, indicating that they are not currently in steady state (Schulz et al., 2017). In such systems, the amount of groundwater in storage is a function of past climate conditions. It is unclear whether this behavior is common to all aquifers containing fossil groundwater recharged under wetter climates than today.

The spatial distribution of ages in a groundwater flow system may be a useful indicator of paleorecharge rates. Recharge rate and travel distance control the mean transit time elapsed since a parcel of groundwater first entered the saturated zone. For an aquifer system dominated by piston flow, groundwater age at a distance of L from the recharge area ($\tau(L)$) is given as:

$$\tau(L) = \frac{L}{v_L} \quad (1)$$

where v_L is the average groundwater velocity since groundwater was recharged (Bethke & Johnson, 2008), which will be controlled by the hydraulic boundary conditions of the system, notably groundwater recharge rate. In a steady-state flow system with uniform hydraulic conductivity and porosity, groundwater age should increase linearly along a flowpath. In a flow system where recharge varied over time, an increase in the spatial gradient of groundwater age would indicate a period of decreased recharge.

Several studies have examined how past climates have affected the distribution of groundwater ages in regional aquifer systems (McCallum et al., 2017; McMahon et al., 2011; Sturchio et al., 2004; Zhu et al., 1998) and employed multiple age tracers that span the full spectrum of expected ages (Markovich et al., 2021; McCallum et al., 2017; Visser et al., 2013). Many studies rely on conventional radioactive age tracers, such as tritium (^3H ; with a half-life [$t_{1/2}$] of 12.32 years) and radiocarbon (^{14}C ; $t_{1/2} = 5,730$ years), which lack the ability to date “intermediate-age groundwater” (~ 100 – $1,000$ years old), as ^3H is useful for dating groundwater < 60 years, while ^{14}C can date waters from $\sim 1,000$ to $40,000$ years old. The use of multiple tracers has revealed that a given packet of groundwater may contain waters of various ages due to hydrodynamic dispersion (Bethke & Johnson, 2008; Suckow, 2014). Without constraints on the distribution of ages, it is difficult to interpret how groundwater flow rates may have varied over time (Ram et al., 2022; Yokochi et al., 2019). Additionally, for the purpose of reconstructing past climate conditions using tracers in groundwater (e.g., stable water isotopes and noble gases), studies that are restricted to a single age tracer (e.g., ^{14}C) often must assume a single “piston flow” recharge age that may be inappropriate for tracer measurements from a groundwater supply well that exhibits substantial mixing of different-aged waters (e.g., Markovich et al., 2021).

Recent advances in analytical measurements of noble gases (Seltzer, Ng, & Severinghaus, 2019) and laboratory and field methodologies (Seltzer, Ng, Danskin, et al., 2019) allow for the reconstruction of past water table depths (WTD) using Kr and Xe isotopes, which record depth-dependent signals of gravitational settling in vadose zone air at the time and place of recharge. Interpreting the timing of past changes in WTD and other paleoclimate indicators, in systems where different tracers reveal that a spectrum of groundwater ages are present in an individual sample, remains a challenge.

We hypothesize that large, regional aquifer systems in the southwestern United States, containing fossil groundwater resources, are a relic of past paleoclimatic conditions and that this may be reflected in groundwater age distributions. Alternatively, recharge to these aquifer systems may have remained relatively constant since the late Pleistocene, leading to generally uniform groundwater age gradients. To assess these competing hypotheses, this study employs five age tracers of varying and overlapping dating timescales, including the relatively rarely used radioactive argon-39 (^{39}Ar ; $t_{1/2} = 269$ years; capable of dating “intermediate age groundwater”), to better characterize groundwater age distributions along a well-defined flow path in the semi-arid Tucson Basin

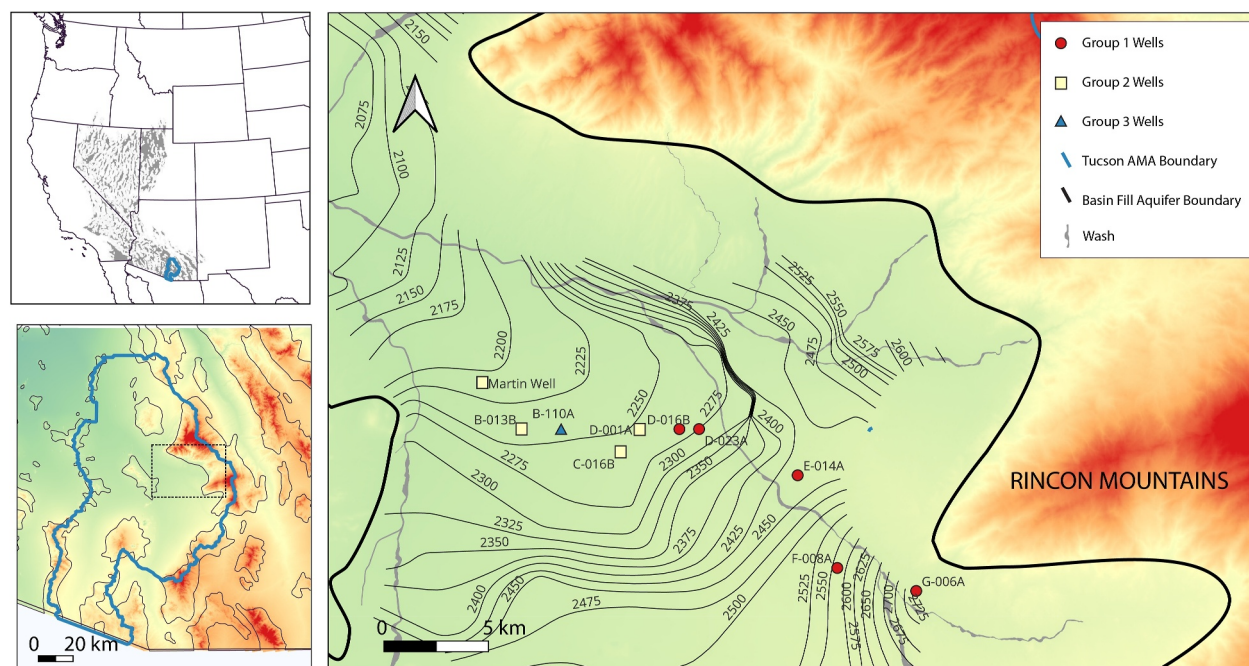


Figure 1. Map of the Tucson Basin showing location of sampled wells in alluvial basin-fill (green shading), major ephemeral and intermittent washes, mountain blocks (red shading with thick black outline), and modern ~25-m water table elevation contours (black lines). The three groups of wells correspond to the following cross-plots. Map on bottom left shows the approximate location of study area (black dotted rectangle) within the Tucson Active Management Area (AMA; blue outline), while map on top left shows the location of the Tucson AMA within the Basin and Range Province in the southwestern US (light gray shading).

(Arizona, USA). Lumped parameter modeling is employed to determine mean groundwater ages to compare to paleo- and hydro-climate proxies. Traditional noble gas measurements are used to infer groundwater recharge temperatures, while krypton (Kr) and xenon (Xe) isotopes are used to reconstruct past WTD (Seltzer, Ng, Danskin, et al., 2019; Seltzer, Ng, & Severinghaus, 2019). Lastly, stable water isotopes ($\delta^{18}\text{O}$ and δD) are used to examine possible changes to the seasonality and mechanisms of recharge (Eastoe & Towne, 2018; Eastoe & Wright, 2019).

The large number of age and climate-sensitive tracers measured in this study provides an opportunity to combine residence time distribution functions with noble gas-derived temperatures and WTD to overcome the substantial mixing of different-aged waters in long-screened groundwater supply wells. We develop and apply an inverse model approach to solve for optimal histories of key hydroclimate parameters over the recharge area, revealing drought conditions in the mid- to late-Holocene with somewhat continuous recharge up until the present.

2. Site Description

2.1. Study Area and Climate

The Tucson Basin, located in southeastern Arizona, is an alluvial basin characteristic of the Basin and Range Physiographic province (Laney, 1972) (Figure 1). The basin is approximately 2,590 km² in size and is bounded by four major mountain ranges: the Santa Catalina Mountains to the north, the Rincon Mountains to the east, the Santa Rita Mountains to the south, and the Tucson Mountains to the west. Average annual precipitation in Tucson is approximately 305 mm (Glueck, 1997); however, greater amounts of precipitation—up to 940 mm—are observed at higher elevations (Ajami et al., 2011). Approximately half of annual precipitation falls during the summer monsoons (July–September) which feature high-intensity, short duration convective storms, while the other half of precipitation is brought during the winter (November–March) through low-intensity, long-duration frontal storms. A portion of this precipitation occurs as snow at high elevations (Ajami et al., 2011). Potential evapotranspiration greatly exceeds annual precipitation by a factor of four to seven (Laney, 1972), even more so during the summer months when solar radiation is more intense.

2.2. Geology

The aquifer transect investigated in this study starts near the base of the Rincon Mountains (Figure 1), which are composed of Precambrian to Neogene age metamorphic and intrusive igneous rocks. The rocks are predominantly granodioritic gneiss and granite, with some felsic to mafic schist and felsic intrusives (Davidson, 1973). Fractures in the granodioritic rocks transmit high elevation precipitation and snowmelt to the base of the mountains where springs occur due to the contact between the crystalline mountain rock and tightly-sealed sedimentary basin fill (Davidson, 1973). The sedimentary deposits of the Tucson Basin comprise the Pantano Formation, Tinaja beds, and Fort Lowell Formation, collectively forming a single aquifer system (Laney, 1972). Due to low porosity and permeability, the Pantano Formation is the least productive basin-fill unit and sparsely tapped for water supplies. Hydraulic conductivity of the lower and middle Tinaja beds is on the order of 3.5×10^{-6} to 7.1×10^{-4} m/s (Davidson, 1973; Hanson & Benedict, 1994; Hanson et al., 1990), while hydraulic conductivity for the upper Tinaja beds is slightly greater and similar to the Fort Lowell Formation, ranging from 1.8×10^{-5} to 2.5×10^{-3} m/s (Hanson & Benedict, 1994; Hanson et al., 1990). The Tinaja beds unconformably overly the Pantano Formation, ranging from 100 m in thickness in much of the basin to over 600 m in the center of the basin, where a triangular-shaped fault-bound depression exists (Laney, 1972). The Fort Lowell Formation is typically 100–120 m thick throughout much of the basin, thinning toward the mountains, and is the most permeable and productive unit in the aquifer (Laney, 1972).

2.3. Hydrology

Prior research has examined recharge mechanisms in the Rincon Mountains (e.g., Olson, 1982; Valentine-Darby et al., 2017), with a more recent study (Eastoe & Wright, 2019) describing three distinct recharge pathways within the mountain block: (a) high-altitude recharge that contains detectable amounts of ^3H , along with a mixed winter and summer stable water isotope signature, that appears to flow through shallow fractures with short residence times; (b) high-altitude recharge with a stable water isotope signature that reflects either equal parts high-altitude winter and summer precipitation, or one that is entirely comprised of precipitation from the 30% wettest summer months; (c) paleo-recharge with a slightly evaporated stable water isotope signature and radiocarbon ages on the order of several thousand years, apparently due to flow through a deeper fracture system. This third component may also be a mixture of ancient precipitation with more recent high-altitude recharge.

In the Tucson Basin, ^3H and ^{14}C measurements have revealed the presence of groundwaters with ages on timescales of decades and millennia (Kalin, 1994). A recent study (Markovich et al., 2021) identified groundwater on the order of 60–290 years old using ^{39}Ar . They discovered that surface mountain front recharge (MFR; infiltration through the basin fill of mountain-sourced perennial and ephemeral stream water after these streams exit the mountain block; Markovich et al., 2019) at the base of the mountains is the dominant recharge component of the basin aquifer system with more limited diffuse mountain block recharge (MBR; subsurface inflow of groundwater to the lowland aquifer that comes directly from the mountain block; Markovich et al., 2019). This discovery was based on residence times, noble gas temperatures, and fluid and energy transport modeling. Recharge from the Rincon Mountains is primarily conveyed to the Tucson Basin by Rillito and Rincon creeks (Eastoe et al., 2004; Eastoe & Wright, 2019). The direction of groundwater flow in the basin is generally northwestward and parallels the surface drainage of the basin (Davidson, 1973).

2.4. Paleoclimate

The U.S. southwest was likely 5–7°C cooler during the late Pleistocene than today based on groundwater isotope and noble gas studies (Kaufman et al., 2020; Phillips et al., 1986; Seltzer, Ng, et al., 2021; Zhu et al., 1998). Recharge was dominated by more winter precipitation leading to paleorecharge rates greater than observed today (Phillips et al., 1986; Seltzer, Ng, et al., 2021; Spaulding et al., 1983; Van Devender & Spaulding, 1979). Paleoclimate in the US southwest has also been examined using numerous other proxies including packrat middens (Holmgren et al., 2006; Spaulding et al., 1983; Van Devender & Spaulding, 1979), tree rings (Faulstich et al., 2012; Meko et al., 2007; Salzer & Kipfmüller, 2005; Woodhouse et al., 2013), lacustrine sediments (LS) (Allen & Anderson, 1993; Krider, 1997; Waters, 1989), and speleothems (Steponaitis et al., 2015; Wagner, 2006; Wong et al., 2015) to assess climatic changes on decadal to millennial timescales.

Many regions of the US southwest experienced a warming trend from the late Pleistocene to the Holocene, with growing evidence of gradual warming globally throughout the Holocene (Osman et al., 2021). Peak aridity is

Table 1
Well Details Including Location, Casing, Screening, Water Table Elevation, and Distance From Recharge

Well	Date sampled	Longitude	Latitude	Elevation (m asl)	Casing bottom elevation (m)	Well screened interval (m asl)	Water table elevation (m asl)	Distance from recharge (km)
G-006A	11/10/2021	−110.73	32.14	882	811	839–811	840	4.8
F-008A	5/11/2021 ^a	−110.77	32.15	878	555	750–561	772	8.5
E-014A	12/3/2020 ^a	−110.79	32.19	848	587	767–600	738	10.5
D-023A	12/3/2020 ^a	−110.84	32.21	804	492	728–492	692	17.1
D-016B	12/3/2020	−110.85	32.21	799	599	714–601	691	17.6
D-001A	12/2/2020 ^a	−110.87	32.21	793	579	732–579	688	18.8
C-016B	12/2/2020 ^a	−110.88	32.20	789	503	649–509	683	19.6
B-110A	12/2/2020 ^a	−110.91	32.21	767	463	633–469	687	22.5
B-013B	12/2/2020	−110.93	32.21	750	582	674–582	681	24.5
Martin	11/12/2021	−110.95	32.23	745	562	693–565	673	26.3

^aDate reflects when ³H was collected; ³⁹Ar was collected at later date.

inferred to have occurred ~6,000 years ago in much of the U.S. southwest (Thompson et al., 1993); however, lake stands from the nearby Willcox Lake (Waters, 1989) may suggest that southeastern Arizona did not desiccate as early. Other lacustrine work (Castiglia & Fawcett, 2006) in northern Mexico shows centennial-scale desiccation cycles with wetter periods occurring around 8.5–8.3 thousand years ago (ka), 6.7–6.1, 4.3–3.8, and 0.2 ka. At this time, climate was approaching the modern regime; however, temperatures were still cooler and there was more rainfall during the summer months (Thompson et al., 1993). Using tree rings, Meko et al. (2007) reconstructed Colorado River flow at Lees Ferry, Arizona, from 762 to 2005 Common Era. Their work shows numerous multi-year and multi-decade droughts over this timespan (e.g., an extreme drought event during the mid-1100s Common Era).

A study conducted in three regions of California (Fresno, the Mojave Desert, and San Diego; to the west of the study area), using Kr and Xe isotopes, demonstrated that WTDs reconstructed for recently recharged waters successfully reproduce modern groundwater levels, while WTDs for the last glacial period (defined as 40–15 ka) were ~18 m shallower compared to today (Seltzer, Ng, Danskin, et al., 2019). They infer that the shallower WTDs encountered during the last glacial period are consistent with other research that suggests the Laurentide Ice Sheet displaced wintertime storms southward, thus delivering more precipitation to the U.S. southwest. At the onset of the Holocene, climatic conditions became more arid, possibly due to the shift in the track of wintertime storms as the Laurentide Ice Sheet retreated (Bromwich et al., 2004; COHMAP Members, 1988; Kulongoski et al., 2009; Lora et al., 2016; Oster et al., 2015).

3. Methods

3.1. Field Methods

Ten wells for drinking water production were sampled between December 2020 and November 2021 along a transect following the current hydraulic gradient from the base of the Rincon Mountains in the east, going northwestward toward the center of the basin (Figure 1). These wells had long screened intervals (Table 1) that draw water from a range of depths and strata within Tucson Basin aquifer system rather than targeting specific hydrostratigraphic units. All wells were operated for at least 1 hr prior to sampling to ensure that at least three well casings of water were purged. All samples were collected from a spigot prior to reaching the storage tank. Temperature, pH, electrical conductivity, and dissolved oxygen were measured at the time of sampling and allowed to stabilize before samples were collected to ensure fresh samples from the aquifer. Samples for alkalinity, anions, and cations were field-filtered through a 0.45 μm nylon filter into pre-cleaned 30 mL high-density polyethylene (HDPE) bottles with minimal headspace. Cation samples were field-acidified with ultra-pure nitric acid to a pH < 2. Samples for δ¹⁸O and δD were collected into 30 mL glass vials with conic tops and no headspace. Unfiltered samples were collected for ³H into 1 L HDPE bottles, carbon-13 (δ¹³C) of dissolved inorganic carbon (DIC) and ¹⁴C into 1 L glass amber bottles, and sulfate isotopes (δ³⁴S-SO₄ and δ¹⁸O-SO₄) into

1 L amber HDPE bottles. All samples were stored on ice in the field and refrigerated in the laboratory to remain at or below 4°C. Traditional noble gases were collected into in-line copper tubes after flushing the tubing with groundwater from the production well and sealing off both ends with metal clamps (Weiss, 1968). Samples for stable Ar, Kr, and Xe isotope measurements were collected into 6-L stainless steel Restek TO air sampling flasks, sealed with a Swagelok SS-4H valves, and weighed on an analog scale to fill to the approximate desired sample weight, following a recently developed headspace-equilibration method (Ng et al., 2023). Samples for ^{85}Kr , ^{37}Ar , and ^{39}Ar required degassing of at least 2 m³ of groundwater in the field using four 3M hydrophobic membranes in parallel and were collected into 61.2 cf. Luxfer industrial aluminum canisters.

3.2. Laboratory Analysis

Alkalinity analysis was performed at the University of Arizona's (UArizona) Department of Hydrology and Atmospheric Sciences and was determined within 24 hr of sampling using the Gran-Alk titration method (Gieskes & Rogers, 1973) with an analytical precision of $\pm 0.6\%$. Anions and cations were measured at the Arizona Laboratory for Emerging Contaminants. Anions (SO_4 , Cl, F, Br, NO_2 , and NO_3) were measured using a Thermo Scientific Dionex ICS-6000 HPIC; analytical precision of $\pm 1\%$ during analysis was observed. Cations (Ca, Mg, Na, K, Si, B) were measured in triplicate using an Agilent 7700x ICP-MS; analytical precision of $\pm 2\%$ across all runs was observed. Charge balances for all samples were within 5%.

$\delta^{18}\text{O}$, δD , ^3H , $\delta^{34}\text{S}\text{-SO}_4$, and $\delta^{18}\text{O}\text{-SO}_4$, and $\delta^{13}\text{C}\text{-DIC}$ analyses were performed at UArizona's Department of Geosciences Environmental Isotopes Laboratory. $\delta^{18}\text{O}$ and δD (‰ VSMOW) were analyzed (precision $< 0.08\%$ and $< 0.9\%$, respectively) using a Finnigan Delta S gas-source isotope spectrometer. ^3H was analyzed using a Quantulus 1220 Spectrometer in an underground counting laboratory using electrolytic enrichment and liquid scintillation decay counting methods (Theodorsson, 1996), with a detection limit of 0.5 tritium units (TU) and analytical precision of $\pm 0.20\text{--}0.21$ TU. $\delta^{34}\text{S}\text{-SO}_4$ (‰ CDT) was analyzed using a ThermoQuest Finnigan Delta Plus XL instrument with an analytical precision of $\pm 0.15\%$. $\delta^{18}\text{O}\text{-SO}_4$ (‰ VSMOW) was analyzed using a Thermo Electron Delta V instrument with an analytical precision of $\pm 0.40\%$. $\delta^{13}\text{C}\text{-DIC}$ was analyzed using a ThermoQuest Finnigan Delta PlusXL coupled with a Gasbench automated sampler with a precision of $\pm 0.2\%$.

^{14}C was analyzed at the NSF-Arizona Accelerator Facility (note: closed fall 2021) using a National Electrostatics Corp. tandem accelerator mass spectrometer with a precision of $\pm 0.10\text{--}0.21\%$ percent modern carbon (pmC); samples collected after the closure of the NSF-Arizona Accelerator Facility (G-006A and Martin Well) were analyzed at the Woods Hole Oceanographic Institution's (WHOI) National Ocean Sciences Accelerator Mass Spectrometry laboratory using NOSAMS's tandem AMS system with a precision of $\pm 0.18\text{--}0.22\%$ pmC.

Noble gases were analyzed at three facilities. He isotopes and noble gas abundance measurements (Ar, Kr, Xe, Ne, ^4He , $^3\text{He}/^4\text{He}$ ratio) were made at the University of Utah's Noble Gas Lab and WHOI's Isotope Geochemistry Facility. At the University of Utah, measurement of all noble gases except helium were completed using a Stanford Research SRS—Model RGA 300 quadrupole mass spectrometer; helium was analyzed using a Mass Analyzers Products—Model 215-50 magnetic sector mass spectrometer. Analytical precision for the gases was Ar ($\pm 2\%$), Kr ($\pm 4\%$), Ne ($\pm 2\%$), Xe ($\pm 4\%$), ^3He ($\pm 1\%$), and ^4He ($\pm 1\%$). At WHOI, noble gases were measured on a WHOI-constructed, statically operated helium isotope mass spectrometer. Helium isotopes were measured using the magnetic sector dual-collecting mass spectrometer to a reproducibility of 0.1%, and the other noble gases using a quadrupole mass spectrometer with a triple mass filter and an electron multiplier operated in pulse counting mode. Analytical precision for the gases was Ar ($\pm 0.1\%$), Kr ($\pm 0.1\%$), Ne ($\pm 0.1\%$), Xe ($\pm 0.2\%$), ^3He ($\pm 0.1\%$), and ^4He ($\pm 0.1\%$). Stable noble gas isotope ratios of Ar, Kr, and Xe were measured in replicate samples at both WHOI and Scripps Institution of Oceanography using a dual-inlet dynamic mass spectrometry approach (Seltzer & Bekaert, 2022; Seltzer, Ng, & Severinghaus, 2019) that facilitates high-precision analyses (≤ 5 per meg $\text{amu}^{-1}/1\sigma$; where 1 per meg = 0.001% = 0.0001%). An inter-lab comparison of noble gas measurements provides high confidence in this method (Ng et al., 2023). Stable noble gas isotope data are reported either as radiogenic ^{40}Ar anomalies ($\Delta^{40}\text{Ar}$; Seltzer, Krantz, et al., 2021) or heavy-isotope enrichment of Kr and Xe ($\delta^*\text{Kr}$ and $\delta^*\text{Xe}$; Seltzer, Ng, Danskin, et al., 2019), relative to atmospheric air. Measurements of ^{85}Kr , ^{37}Ar , and ^{39}Ar activities were performed in the Deep Low Level Counting Laboratory of the Physics Institute, University of Bern, Bern, Switzerland. Prior to the activity measurements pure Ar and Kr fractions were separated from the bulk gas using large volume gas chromatography (GC) methods. Following separation, samples were measured for ^{85}Kr , ^{37}Ar , and ^{39}Ar using ultra-low β -decay counting (Loosli, 1983; Riedmann & Purtschert, 2016).

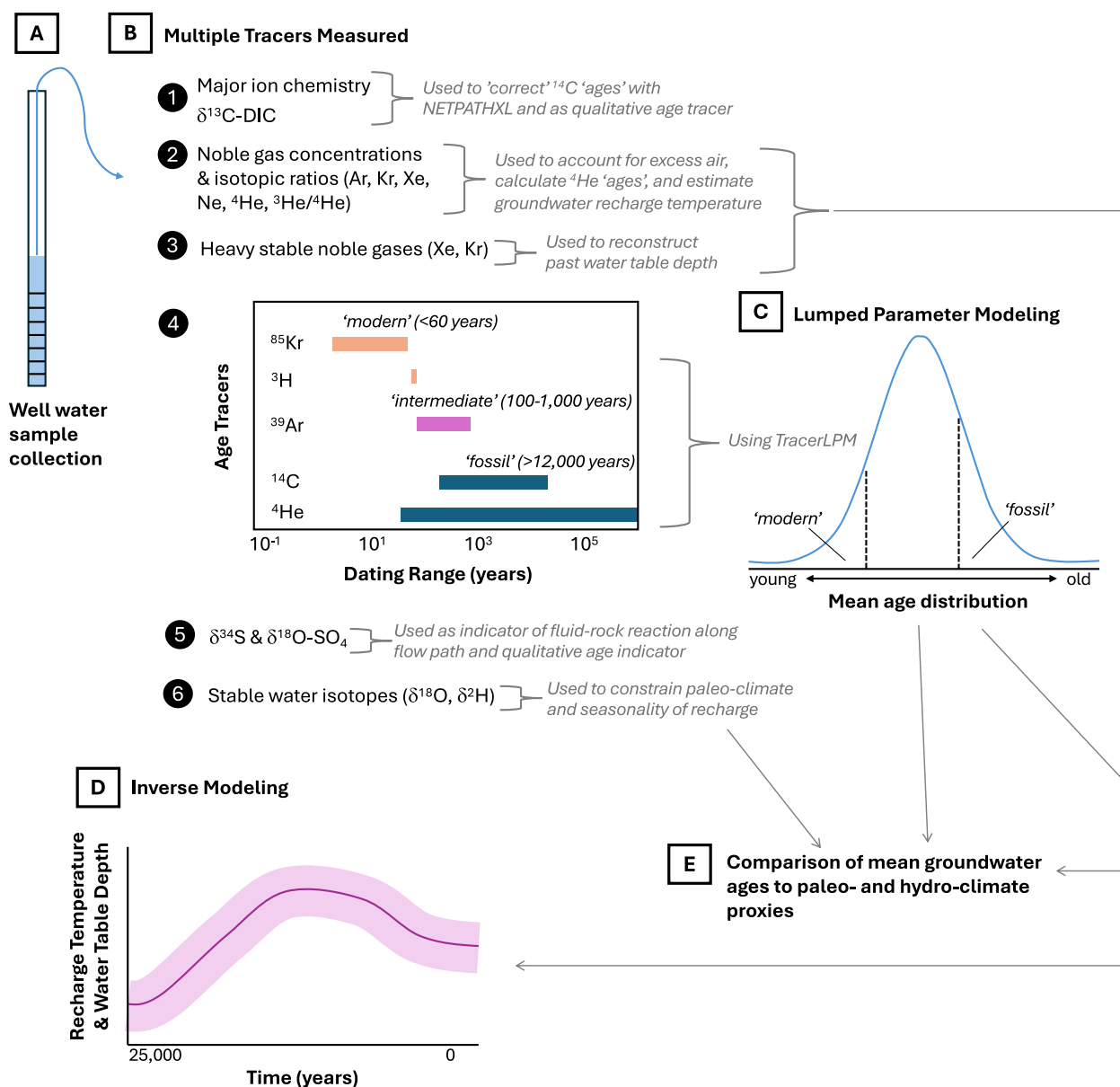


Figure 2. Schematic diagram of multi-tracer approach utilized in this study to reconstruct mean age distribution, paleo-recharge temperature, and water table depth of groundwater along the sampled flowpath and compare with other paleo- and hydro-climate proxies (e.g., stable water isotopes).

3.3. Tracer Interpretations

The overarching conceptual approach we employ in this study is to view all measured tracers in sampled groundwater wells (listed in Figure 2, “A” and “B” steps) as reflecting mixtures of water parcels of varying residence time. In this sense, tracer signals that record variations of recharge parameters (e.g., noble gas temperature, water table depth, and stable water isotopes) over time, for example, due to climatic and/or hydrogeological change, have been smoothed by mixing. Our approach operates in two main steps to deconvolve recharge signals and mixing. The first step is to employ a combination of measured age tracers to constrain the distribution of groundwater ages reflected by a single sample via lumped parameter modeling (LPM; labeled “C” in Figure 2). The second is to “unmix” climatic or hydrogeologic tracer signals (e.g., noble gas temperature) by combining tracer measurements and age-tracer-informed residence time distributions in an inverse model (“D” in Figure 2). The result of this analysis is to estimate the temporal history of climate and hydrogeology in the recharge area of the aquifer, using all available tracer data from each well (“E” in Figure 2). Here we briefly

describe the conceptual treatment of tracer data, before detailing the LPM and inverse modeling approach in Section 3.4.

^{14}C values were corrected to account for geochemical reactions occurring in the subsurface—e.g., carbonate mineral dissolution—that impact ^{14}C activity by the addition of “dead carbon” (0 pmC ^{14}C), artificially increasing the apparent groundwater age (Clark & Fritz, 1997). NetpathXL (Parkhurst & Charlton, 2008), a revised version of NETPATH (Plummer et al., 1994) which employs inverse geochemical models, was used to make these corrections and included measured major ion chemistry (alkalinity, cations, anions) and $\delta^{13}\text{C}$ -DIC values (Figure 2). The model assumptions, mineral phases, and constraints that were used are based on past investigations in the Tucson Basin (Kalin, 1994; Markovich et al., 2021; Parada et al., 1983). Assumed values for ^{14}C (105 pmC) and $\delta^{13}\text{C}$ of soil CO_2 (−18.3‰) and ^{14}C (5 pmC) and $\delta^{13}\text{C}$ of local carbonates (−3.5‰) also came from these previous investigations (Kalin, 1994; Parada et al., 1983) and are typical of semi-arid regions. Mineral constraints included measured carbon, sulfur, calcium, magnesium, sodium, potassium, chloride, and silica concentrations. Phases included CO_2 gas, biotite, calcite, gypsum, Mg-montmorillonite, silica, sodium chloride, albite, and proton exchange. Forced dissolution of CO_2 gas and biotite was used following Kalin (1994) and Markovich et al. (2021). Proton exchange (e.g., Appelo, 1994) was included to account for $\delta^{13}\text{C}$ -DIC values of samples exceeding incongruent dissolution of calcite, as used in previous NETPATH modeling in the Tucson and adjacent basins (Hopkins et al., 2014; Kalin, 1994; Markovich et al., 2021). Isotope exchange of calcite was employed, based on observations from Kalin (1994), to account for dissolution and recrystallization of calcite in the aquifer that can also modify the $\delta^{13}\text{C}$ -DIC signature of groundwater. Enrichment of Na through cation exchange with clays and increasing $\delta^{34}\text{S}$ and $\delta^{18}\text{O}$ of SO_4 from gypsum dissolution was used as a qualitative indicator of residence time (i.e., evidence of greater fluid-rock reaction, as previously seen in the Tucson, Eastoe et al., 2004 and adjacent Middle San Pedro alluvial basins, Hopkins et al., 2014) to support the more quantitative age tracer results (Figure 2, “b”).

To account for noble gas concentrations in excess of equilibrium solubility (i.e., excess air) and to calculate environmental parameters temperature (T), salinity (S), and pressure (P), many different correction models have been formulated over the years as reviewed in Aeschbach-Hertig and Solomon (2013). This study used PANGA (Jung & Aeschbach, 2018) to perform a χ^2 minimization with 10,000 Monte Carlo realizations to solve for T, dissolved excess air (A), and equilibrium concentrations using the closed-system equilibrium (CE) model (Aeschbach-Hertig et al., 2000; Jung et al., 2013), based on the measured values of S, P, Ne, Ar, Kr, and Xe. The CE model was chosen over other correction models for several reasons: the parameters capture physical conditions during gas exchange, noble gases tend to exhibit CE-type fractionation (Kipfer et al., 2002), the CE model has been shown to outperform other leading models for accuracy and goodness of fit with Holocene-age samples (Seltzer, Ng, et al., 2021), and the CE model was successfully employed by Markovich et al. (2021) in their nearby, recent study. Finally, WTD were reconstructed using an inverse model based on the relationship between Kr and Xe isotope ratios detailed in Seltzer, Ng, Danskin, et al. (2019) (Figure 2, “D”). Stable water isotopes were used to infer past hydroclimate, including changes in precipitation sources and seasonality over geologic time (e.g., Eastoe, 2023), when compared to corrected mean groundwater age (Figure 2, “E”).

To use ^4He as an age tracer, concentrations were differentiated between atmospheric, in situ, and potential external (i.e., crustal and/or mantle) inputs. Equations and various assumptions used are detailed at length by Craig and Lupton (1976), Torgersen (1980), Torgersen and Clarke (1985), Hilton (1996), Ballentine et al. (1996), Castro et al. (2000), Ballentine and Burnard (2002), and Saar et al. (2005) (Appendix A in Supporting Information S1). The in situ production rate of radiogenic ^4He was determined following the equations presented in Supporting Information S1 (Ballentine & Burnard, 2002; Ballentine et al., 1996; Castro et al., 2000; Craig & Lupton, 1976; Hilton, 1996; Saar et al., 2005; Torgersen & Clarke, 1985) and using aquifer properties of density and porosity for the Tucson Basin (Davidson, 1973), while uranium (U) and thorium (Th) were estimated based on aerial gamma-radiation and geology data sets (Jurgens et al., 2012; Phillips et al., 1993; Reed & Bush, 2005), resulting in values consistent with Markovich et al. (2021).

3.4. Lumped Parameter Modeling and Inverse Model Approach to Reconstruct Recharge Temperature and Water Table Depth

To account for mixing of groundwater from multiple flow paths, USGS software TracerLPM (Jurgens et al., 2012) was used to create LPMs (Figure 2, “C”). A detailed explanation of how TracerLPM was employed to

generate LPMs is provided in Appendix B in Supporting Information S1. Following Markovich et al. (2021), several LPMs were considered for this study including the piston flow model, exponential mixing model, and a binary mixing PFM-EMM model. Diagnostic tracer-tracer plots in TracerLPM were used to visually assess which of the models fit best to measured tracer concentrations with the lowest relative error (Figures S5–S12 in Supporting Information S1). Once a model was selected, TracerLPM was used to perform closed form analytical solutions for probability density function and cumulative density functions of groundwater age in each of the individual wells. Finally, mean age was determined using a χ^2 minimization function.

LPM analysis indicates that there is substantial mixing of different aged-waters in the supply wells sampled in this study (Figure S1 in Supporting Information S1). To disentangle climatic changes from mixing, we apply an inverse model that solves for an optimal time history of a given parameter, which in this study are either (a) noble gas temperature [NGT] or (b) $\delta^*\text{Xe}$ [a proxy for WTD] (Figure 2, “D”). As described in Section 3.3, NGTs were calculated using the CE model, which uses measured Ne, Ar, Kr, and Xe to solve for NGT along with entrapped air, A, and its partial dissolution (or fractionation), F. We refer the reader to Aeschbach-Hertig et al. (2000) for the original CE model. For the mixing deconvolution analysis in this study, we assume that NGT is a conservative parameter with respect to mixing, and we demonstrate the validity of this assumption through a simple numerical experiment in which temperature and noble gases in warm and cold water masses are mixed to varying extents. We find that apparent NGTs (calculated with the CE model) agree closely with actual NGTs, to within 1°C in even the most extreme of mixing scenarios (Figure S2 in Supporting Information S1). Thus, NGT is treated as a “mixable” property for the purpose of the inverse modeling approach of this study.

Stable Xe isotopes are used in this study to infer WTD at the time and place of recharge. We adopt the parameter $\delta^*\text{Xe}$ (Seltzer, Ng, Danskin, et al., 2019), which is a mass-difference-normalized, error-weighted mean of six stable Xe isotope ratios ($^{136}\text{Xe}/^{129}\text{Xe}$, $^{134}\text{Xe}/^{129}\text{Xe}$, $^{132}\text{Xe}/^{129}\text{Xe}$, $^{131}\text{Xe}/^{129}\text{Xe}$, $^{130}\text{Xe}/^{129}\text{Xe}$, and $^{128}\text{Xe}/^{129}\text{Xe}$), reported as a per meg (i.e., part per million) per mass unit (i.e., amu), deviation from the atmospheric Xe isotope composition. Briefly, heavy noble gas isotopes (Kr and Xe) dissolved in groundwater retain an isotopic signal imparted by gravity in soil air, which leads to greater enrichment in heavy isotopes (i.e., increasing $\delta^*\text{Xe}$) with greater WTD (Seltzer, Ng, Danskin, et al., 2019). In this study, both Kr and Xe isotopes were measured and reported, but because both display extremely close agreement with gravitational settling theory (Figure S3 in Supporting Information S1, Section 4.4), only $\delta^*\text{Xe}$ is used in the inverse modeling approach. While the inverse model explicitly solves for an optimal time history of $\delta^*\text{Xe}$, we discuss the inferred WTD history by making use of gravitational settling theory, whereby $\delta^*\text{Xe}$ is equal to WTD (in m) times the theoretical gravitational settling slope of 4 per meg $\text{amu}^{-1} \text{m}^{-1}$ plus the contribution of solubility equilibrium fractionation (ϵ_{sol}), tightly constrained by prior work to be 21 ± 2 per meg amu^{-1} between 10 and 20°C (Seltzer, Ng, & Severinghaus, 2019; Seltzer et al., 2023). Thus, WTD can be calculated, to close approximation, via the following relation:

$$\text{WTD (m)} = (\delta^*\text{Xe} - \epsilon_{\text{sol}}) / 4 \quad (2)$$

The inverse model solves for an optimal time history of two parameters of climatic and hydrogeologic interest in the recharge area: recharge temperature (recorded by NGT) and water table depth (recorded by $\delta^*\text{Xe}$). This approach estimates time histories of NGT or $\delta^*\text{Xe}$ via nonlinear least squares, using an interior-point method implemented by MATLAB's *fmincon* solver. Specifically, the inverse problem is set up to minimize a cost function that represents the squared deviation of measured and modeled parameter values across all 10 Tucson Basin wells, in Equation 2:

$$\text{CF} = \sum_{i=1}^{10} \left(\frac{x_{\text{mod}} - x_{\text{meas}}}{x_{\text{meas}}} \right)^2 \quad (3)$$

where x is the parameter of interest (either NGT or $\delta^*\text{Xe}$) and the subscripts mod and meas refer to modeled and measured values, respectively. The model estimates each x_{mod} value by integrating the product, a modeled time series of variable x , with the age distribution function of a given well, $G(t)$. $G(t)$ reflects the probability distribution of groundwater residence time—that is, the fractional contribution of different aged waters—in a sample from a groundwater well. Conceptually, this integration directly accounts for the impact of mixing on measured values in groundwater samples, because $G(t)$ reflects the mixture of different aged water comprising a given sample. Formally, the model calculates x_{mod} for each well in Equation 3 as:

$$x_{\text{mod}} = \int x(t) \cdot G(t) dt \quad (4)$$

where $x(t)$ is the time series of a given parameter in the recharge area of the aquifer (either NGT or $\delta^*\text{Xe}$). The forward model $x(t)$, is computed by interpolating values of a given recharge parameter (NGT or $\delta^*\text{Xe}$) at five points in time: Late Holocene (0 ka), Mid Holocene (5 ka), Early Holocene (10 ka), LGM (20 ka), and a long-term well-mixed end-member reflecting the small portion of recharge prior to 40 ka that may exist in some wells. Thus, the inverse model solves for only five parameters: the values of x at each of the time points. The product, $x(t)$, a modeled time series of variable x , is interpolated between 0 and 20 ka by cubic spline interpolation using MATLAB's `interp1` routine. The LGM parameter value is assumed to prevail between 20 and 40 ka, and the long-term mixed value prevails for all time points prior to 40 ka. The choice of five age points and a long-term mixed value is made to avoid overfitting and in consideration of the large extent of mixing of different aged waters suggested by the age distribution functions, $G(t)$, for the oldest and most downgradient wells.

The optimization routine applies basic physical constraints, such that NGTs must be above freezing (0°C) and below 30°C , and WTD must be positive (i.e., below ground, $\delta^*\text{Xe} > 28$ per meg amu^{-1} of air-equilibrated water). For each parameter, 100 Monte Carlo simulations were run in which random errors (equal to 1σ uncertainties) are added to measured values for the purpose of estimating uncertainty in the inverse model solution. The model reports the mean and 95% confidence interval of the time series $x(t)$ found by these Monte Carlo simulations for each parameter. Note that for $\delta^*\text{Xe}$, Equation 4 was modified such that the $\delta^*\text{Xe}$ time series is weighted by the inverse of the optimal NGT history (since colder water contributes more Xe to a mixture, owing to the inverse temperature dependence of Xe solubility in water):

$$\delta^*\text{Xe}_{\text{mod}} = \frac{\int \delta^*\text{Xe}(t) \cdot [\text{Xe}](t) \cdot G(t) dt}{\int [\text{Xe}](t) dt} \quad (5)$$

where $[\text{Xe}](t)$ is the time history of Xe concentration at the time and place of recharge. This weighting is needed to reflect that colder water holds more Xe and thus contributes more to a mixture, relative to warmer water.

To demonstrate and evaluate the behavior of the inverse model, we carried out a simple numerical experiment using synthetic data, in which “samples” were drawn from a series of hypothetical wells that experienced substantial mixing of different-aged waters. The inverse model, informed only by synthetic noble gas data and age distributions for the wells, was able to faithfully capture the prescribed temperature history in the recharge history, despite the extensive smoothing of apparent NGTs due to mixing. Appendix D in Supporting Information S1 describes this numerical experiment in more detail.

This coupled lumped parameter-inverse model approach represents an advance in providing a new framework for deconvolving paleoclimatic tracer time histories from mixing in groundwater that is heavily impacted by mixing of different-aged waters, and it incorporates uncertainties from analytical measurements and noble gas modeling through Monte Carlo simulations. However, it does not explicitly account for uncertainty in the lumped parameter model-based groundwater residence time distribution functions. We discuss this limitation and others, while providing a quantitative evaluation of the inverse model, in Section 5.3.

4. Results

4.1. Field Parameters and Major Ions

Water quality parameters, alkalinity, and major ions of groundwater samples were measured at all 10 production wells across the transect (Table 2). Temperature ranged from 18.5 to 35.3°C , pH ranged from 6.95 to 8.65, and conductivity ranged from 219 to 435 $\mu\text{S}/\text{cm}$, generally increasing downgradient from southeast at the base of the Rincon Mountains toward the center of the basin to the northwest. Alkalinity was lowest (85.8 mg/L) in the recharge area well (G-006A), then remained generally consistent across the rest of the transect, ranging from 121 to 139 mg/L. Given that all samples had a $\text{pH} < 9$, bicarbonate (HCO_3^-) is assumed to be the dominant constituent of alkalinity. Most samples are characterized as Mg- HCO_3 type waters. Wells C-016B, B-110A, and Martin Well have a mixed-type signature with greater concentrations of Na; B-013B was also a mixed-type water but was dominated by SO_4 and had the highest TDS (320.5 mg/L). Additionally, all samples contained detectable levels of

Table 2
General Ion Chemistry and Water Quality Parameters

Well	Ca	Mg	Na	K	Si	B	F	Cl	Br	HCO ₃	SO ₄	NO ₃	pH	Temp (°C)	EC (μS/cm)
G-006A	29.6	2.83	11.5	0.93	12.2	0.011	0.14	4.73	0.20	85.8	12.7	6.13	6.95	18.5	219
F-008A	36.7	4.25	14.7	1.22	12.2	0.011	0.16	4.80	0.16	134	12.3	13.1	7.71	22.3	287
E-014A	29.2	2.00	23.3	1.32	15.2	0.024	0.14	4.40	0.20	131	14.7	8.09	7.72	27.3	289
D-023A	28.0	1.55	23.9	1.55	16.3	0.027	0.10	5.46	0.20	139	19.1	9.60	7.69	28.5	311
D-016B	25.1	1.97	22.6	1.27	14.8	0.032	0.13	4.58	0.21	131	8.77	5.53	7.79	28.3	262
D-001A	22.3	1.14	26.5	1.26	15.0	0.036	0.15	3.78	0.20	134	6.35	3.48	8.31	29.1	247
C-016B	18.5	1.12	30.2	1.41	15.6	0.040	0.15	7.17	0.21	132	18.9	4.00	8.24	30.1	284
B-110A	13.1	0.39	53.8	1.78	15.6	0.057	0.23	5.69	0.19	121	47.1	1.24	8.65	35.3	349
B-013B	35.3	2.75	43.8	2.15	15.3	0.044	0.17	11.3	0.25	134	69.8	5.53	7.60	29.7	435
Martin	30.4	0.83	52.8	1.88	14.6	0.053	0.21	8.29	0.20	131	55.2	4.18	7.77	30.0	406

Note. Units in mg/L for all analytes, except for pH, Temperature (Temp), and Electrical Conductivity (EC).

NO₃ ranging from 1.24 to 13.1 mg/L, with concentrations generally decreasing along the transect from southeast to northwest.

4.2. Stable Isotopes

Stable water isotope values ranged from -7.7 to -10.5‰ and -54.9 to -79.5‰ for $\delta^{18}\text{O}$ and δD , respectively (Table 3; Figure 3). All samples plotted below the average Local Meteoric Water Line (LMWL) for Tucson, as well as LMWLs that are weighted for summer-dominant and winter-dominant precipitation (Eastoe & Dettman, 2016). In fact, most samples generally plotted along the Global Meteoric Water Line (GMWL) where $\delta\text{D} = (\delta^{18}\text{O} \times 8.0) + 10$, as reported in Craig (1961). Samples $\delta^{18}\text{O}$ and δD values range from above modern summer precipitation, mean weighted (for 30% wettest months) at mid-elevation (1,400 m above sea level) in the Rincon Mountains (Eastoe & Wright, 2019), to near winter precipitation, although relatively depleted in ^2H . Given the strong correlation between $\delta^{18}\text{O}$ and δD of the samples ($R^2 = 0.9013$; $P = 3.46 \times 10^{-10}$), further discussion of stable water isotopes will be limited to $\delta^{18}\text{O}$.

Stable carbon isotope values of DIC ($\delta^{13}\text{C}$ -DIC) ranged from -8.9 to -14.3‰ (Table 3), generally increasing from southeast to northwest along the direction of groundwater flow. Stable sulfur and oxygen isotope values of sulfate ranged from $+3.8$ to $+12.6\text{‰}$ and $+6.2$ to $+19.5\text{‰}$ for $\delta^{34}\text{S}$ -SO₄ and $\delta^{18}\text{O}$ -SO₄, respectively (Table 3), with $\delta^{34}\text{S}$ -SO₄ generally increasing along the direction of groundwater flow (Figure S4 in Supporting Information S1).

Table 3
Stable Isotopes

Well	$\delta^{18}\text{O}$ (‰)	δD (‰)	$\delta^{34}\text{S}$ -SO ₄ (‰)	$\delta^{18}\text{O}$ -SO ₄ (‰)	$\delta^{13}\text{C}$ -DIC (‰)
G-006A	-9.4	-65.3	3.8	11.3	-14.3
F-008A	-9.6	-66.7	4.9	16.0	-12.5
E-014A	-9.3	-65.6	5.6	19.5	-12.3
D-023A	-9.3	-64.7	8.4	10.8	-12.6
D-016B	-9.7	-67.1	7.3	9.9	-11.8
D-001A	-8.8	-60.3	5.0	6.2	-11.5
C-016B	-8.4	-58.8	9.9	8.7	-10.6
B-110A	-10.5	-79.5	11.8	12.3	-8.9
B-013B	-7.7	-54.9	12.6	18.9	-10.2
Martin	-8.0	-58.3	12.5	6.3	-9.1

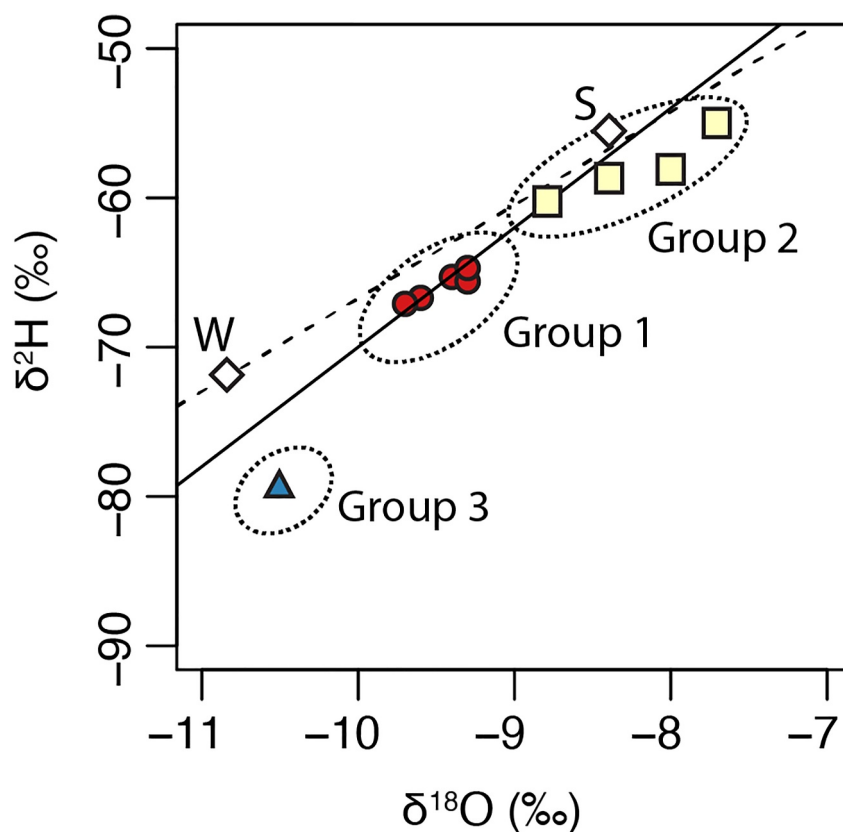


Figure 3. Stable water isotope values of well water samples relative to the Global Meteoric Water Line (solid black line) (Craig, 1961) and Local Meteoric Water Line (dashed black line) (Eastoe & Dettman, 2016). Weighted mean summer (S) and winter (W) precipitation from 30% wettest months at 1,400 m elevation above sea level in the Rincon Mountains shown in diamonds for reference (Eastoe & Wright, 2019). Refer to text for identification of three groups.

4.3. Radioactive and Radiogenic Isotope Age Tracers

Tritium was detected at G-006A (2.6 ± 0.2 TU), F-008A (0.9 ± 0.2 TU), and B-110A (<0.7 TU; apparent 0.3 ± 0.21 TU) (Table 4). The apparent ^3H detection (0.3 ± 0.21 TU) at B-110A is less than the method detection limit (0.5 TU). Repeat ^3H sampling was conducted at F-008A and B-110A, approximately six months and 11 months later, respectively. F-008A (1.0 ± 0.21 TU) still contained detectable ^3H similar to the previous measurement and B-110A (non-detected) confirmed the previous measurement was likely spurious. For the purposes of dating, an average value of 0.95 TU is used for F-008A. At all remaining wells, ^3H was below the detection limit.

^{85}Kr was detected in four of six samples, ranging from 2.6 to 17.1 dpm/cm³ Kr, translating to ^{85}Kr ages of 24–53 years (Table 4). ^{39}Ar ranged from 12 to 60% modern argon (pmA), with ^{39}Ar ages ranging from 210 to 820 years (Table 4; Figure 4a). ^{14}C was detected in all samples with uncorrected ^{14}C ranging from 7.8 to 104.9 pmC. Corrected ^{14}C “ages” ranged from 0.23 to 16.5 ka, generally increasing along the transect from southeast to northwest, following the direction of groundwater flow (Figure 4b). Excluding B-110A, which is substantially older (16.5 ka) than other samples, corrected ^{14}C ages ranged from 0.23 to 7.3 ka (Table 4). Radiogenic ^4He was detected in seven of the wells, with ^4He ages ranging from 1.8 to 35.6 ka (Table 4) (Figure 4c), generally consistent with corrected ^{14}C ages; ^4He and ^{14}C ages only differed by a factor of 0.79–3.20, suggesting no substantial external ^4He flux, from deeper sources, in the area. Mean groundwater ages, based on LPMs, ranged from 0.15 to 29.5 ka (Table 4) (Figure 4d). Mean groundwater ages were younger than corrected ^{14}C ages at three wells and older than corrected ^{14}C ages at the remaining seven wells, differing by a factor of 0.64–2.56.

Table 4
Radioactive Isotopes and Age Tracers

Well	³ H		⁸⁵ Kr dpm/cm ³ Kr	⁸⁵ Kr Years	³⁹ Ar		¹⁴ C pmC	¹⁴ C age (corrected) ka	⁴ He age ka	Mean age ka
	TU	Years			pmA	ka				
G-006A	2.6	11.6	—	—	—	—	105	0.23	—	0.15
F-008A	0.95	29.5	17.1	24	58	0.21	83	0.26	—	0.34
E-014A	<0.5	—	5.6	40	59	0.21	60	2.3	3.3	2.9
D-023A	<0.5	—	2.6	53	44	0.32	59	2.3	1.8	1.6
D-016B	<0.5	—	—	—	—	—	59	2.4	—	2.4
D-001A	<0.5	—	4.4	45	60	0.20	36	6.3	10.1	8.8
C-016B	<0.5	—	ND	—	34	0.42	31	7.3	23.4	19.8
B-110A	<0.5	—	ND	—	12	0.82	8	16.5	35.8	29.5
B-013B	<0.5	—	—	—	—	—	36	5.1	13.7	11.8
Martin	<0.5	—	—	—	—	—	28	7.3	20.2	17.0

Note. ND = non-detected. pmA = percent modern Argon.

4.4. Noble Gases

Across wells sampled in this study, ³He/⁴He ranges from 0.25 to 1.04 Ra (where 1 Ra = 1.34×10^{-6} , the atmospheric ³He/⁴He ratio), with values near atmospheric (i.e., ~1) at the mountain front in the area of modern recharge, and lower values (e.g., 0.25) further along the flow path and deeper in the basin, indicating accumulation of radiogenic ⁴He (Table 5). ΔNe ranged from 28% to 322%, suggesting an excess air component present in many samples. ⁴He_{rad} was present in seven of 10 wells, ranging from 6.93×10^{-9} – 1.38×10^{-7} , indicative of either an excess source of ⁴He and/or longer residence time. The CE-model (Aeschbach-Hertig et al., 2000) was run unconstrained with P set to an approximate modern recharge elevation of 1,140 m. Model results produced χ^2 values (0.02–3.9) and associated probabilities (Pr; 4.86%–90.1%) that fit the data well (Table 5). Apparent NGTs from individual wells ranged from 10.6 to 19.6°C (Table 5; Figure S1 in Supporting Information S1).

All 10 wells analyzed in this study show clear evidence of gravitational enrichment of heavy Kr and Xe isotopes (Figure S3 in Supporting Information S1, Table 6), with highly correlated δ*Kr and δ*Xe values ($R^2 = 0.95$) close to the theoretical gravitational settling slope of 1 (Seltzer, Ng, Danskin, et al., 2019). Apparent WTD for each well ranges from 6.35 to 38.47 m (Table 5), based on Kr and Xe isotopes and applying the WTD reconstruction approach of Seltzer, Ng, Danskin, et al. (2019). NGT and WTD from individual wells show an apparent inverse relationship, with a peak in apparent recharge temperature coupled with a maximum in WTD observed near the late-Holocene (Figures 5b and 5c), but our ability to interpret individual-well values is hampered by the wide residence time distribution functions induced by mixing (e.g., Figure S1 in Supporting Information S1).

We therefore apply our inverse model approach to solve for optimal histories of both NGT and WTD at the recharge site, using measured noble gas abundances, isotope ratios, and LPMs constrained by multiple age tracers (Figure 6). Recharge-site histories of NGT and WTD show maximum values near the mid-Holocene (Figures 6a and 6c). The inverse model approach suggests a recharge temperature in the mid-Holocene that is close to the modern mean annual surface temperature (MAST) in the Tucson region at 1,140 m ($20.6 \pm 0.9^\circ\text{C}$) based on ERA5-Land reanalysis data (Hersbach et al., 2020), coinciding with the deepest WTD (Figure 6). However, the inverse model suggests both colder recharge temperatures and shallower WTD before and after the mid-Holocene, consistent with observations of colder-than-MAST groundwater (18.5°C) during sampling at the furthest upgradient well (G-006A). This implies a decoupling between MAST and recharge temperature during periods with shallower WTD (and likely greater recharge), which we attribute to advection of cold mountain front recharge (Markovich et al., 2021) and discuss in Section 5.

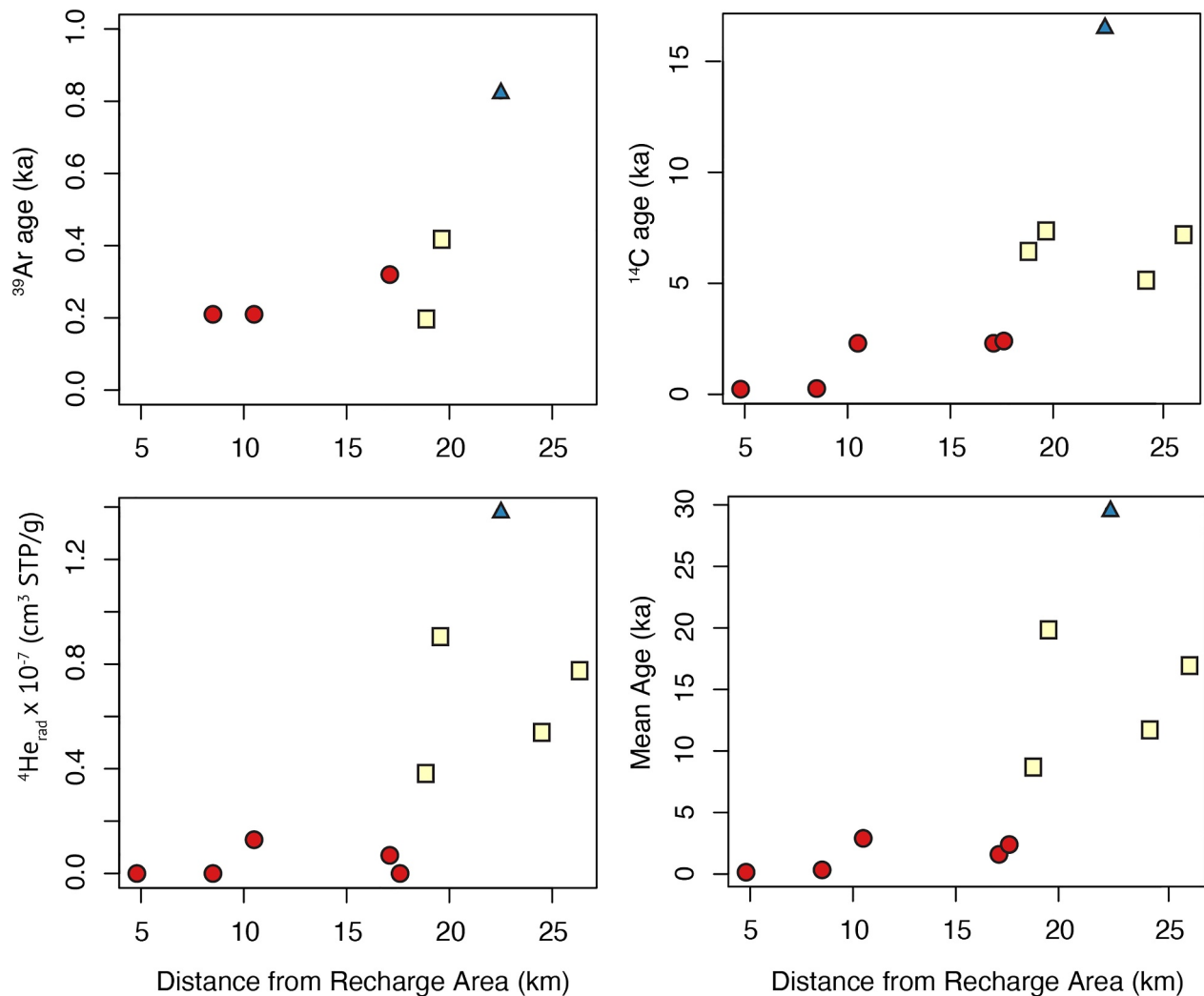


Figure 4. From top left to right: plots of (a) ^{39}Ar age (ka), (b) corrected ^{14}C age (in thousands of years, ka), (c) $^4\text{He}_{\text{rad}} (\times 10^{-7} \text{ cm}^3 \text{ STP/g})$, and (d) mean groundwater age (ka) vs. distance from recharge area. Symbology of wells corresponds to three groups in Figure 3.

5. Discussion

5.1. Groundwater Residence Times

Groundwater residence times that generally steadily increase with distance along inferred groundwater flow paths indicate that the Tucson Basin has been receiving somewhat continuous recharge since the Pleistocene Epoch. Simultaneous detections of ^3H , ^{85}Kr , ^{39}Ar , ^{14}C , and $^4\text{He}_{\text{rad}}$ in some of the wells demonstrate a mixed groundwater age distribution that reflects recharge on decadal, centennial, and millennial timescales. Additionally, concurrent detections of multiple tracers at most of the wells demonstrates that groundwater is comprised of a mixture of multiple flow paths as expected from long-screened production wells. The general progression in groundwater ages with distance from the recharge area is accompanied by increases in TDS, alkalinity, and $\delta^{34}\text{S-SO}_4$ values (Tables 2 and 3), reflective of greater water-rock interaction (i.e., carbonate and evaporite mineral dissolution) along the flow path.

The presence of ^3H in wells G-006A and F-008A indicates modern recharge at the mountain front, and limited diffuse recharge across the basin, as shown in past studies of the Tucson Basin (Eastoe et al., 2004; Kalin, 1994; Markovich et al., 2021). Excluding upgradient well F-008A, ^{85}Kr detection in the downgradient wells suggests a component of groundwater on the order of 40–53 years old, which is consistent with the non-detection of ^3H in those wells; the theoretical dating limit for ^3H is the early 1950s (the beginning of major

Table 5*Noble Gas Data, Closed-System Equilibrium Model Results (X^2 , Pr (χ^2) %) Paleotemperature of Recharge and Reconstructed Water Table Depth (WTD)*

Well	^3He 10^{-14}	^4He 10^{-8}	$^4\text{He}_{\text{rad}}$ 10^{-8}	Ne 10^{-7}	Ar 10^{-4}	Kr 10^{-8}	Xe 10^{-8}	X^2	Pr (χ^2) %	T ($^{\circ}\text{C}$)	WTD (m)
G-006A	9.38	6.58	–	3.68	3.38	7.15	0.96	3.9	4.86	17.1	10.95
F-008A	26.7	18.6	–	7.14	5.71	10.2	1.21	1.4	24.4	15.6	16.41
E-014A	6.38	6.73	1.29	2.13	3.19	6.91	0.94	0.26	61.0	17.2	17.62
D-023A	7.62	6.11	0.69	2.11	3.01	6.47	0.87	0.04	84.5	19.6	38.47
D-016B	9.10	6.90	–	2.76	3.22	6.91	0.94	0.52	47.1	17.4	27.12
D-001A	9.31	10.4	3.88	2.42	3.43	7.23	0.96	0.06	80.2	17.5	17.02
C-016B	9.97	16.4	9.02	2.68	3.59	7.58	1.01	0.09	75.8	16.0	21.89
B-110A	7.43	21.6	13.8	2.90	3.93	8.55	1.19	0.06	81.1	10.6	6.35
B-013B	10.7	14.4	5.29	3.34	3.64	7.64	1.03	0.02	90.1	15.0	20.89
Martin	8.94	15.2	7.79	2.71	3.46	7.48	1.02	0.06	80.8	14.9	19.41

Note. Concentrations for ^3He , ^4He , $^4\text{He}_{\text{terr}}$, Ar, Kr, Ne, Xe, and A are cm^3 STP/g. See methods section for analytical error associated with noble gases. Additional noble gas data in Table 6.

nuclear bomb testing), given the analytical detection limit of 0.5 TU. At the one location where both tracers were detected (F-008A), calculated ^3H and ^{85}Kr ages are similar.

Depleted ^{39}Ar below the modern value of 100 pmA at all six wells sampled provides evidence of intermediate-age groundwater (210–820 years) throughout much of the basin. In a transect northeast of the current study area, Markovich et al. (2021) also identified centuries-old groundwater with ^{39}Ar ages ranging from modern to 290 years but with ^3H detected in most wells. The generally younger groundwater ages are likely due to the closer proximity to the Santa Catalina Mountains and prominent washes where modern recharge occurs. The results of this study and Markovich et al. demonstrate that recharge in the northeast and east portions of the Tucson Basin has been occurring fairly continuously from at least ~820 years ago to the present.

Corrected ^{14}C ages (0.23–16.5 ka) and increasing concentrations of $^4\text{He}_{\text{rad}}$ with depth and distance along the flow path indicates the presence of an older groundwater component on millennial age scales (Solomon, 2000). The generally older mean groundwater ages (0.15–29.5 ka) compared to corrected ^{14}C ages are reflective of the bias in apparent age toward the younger groundwater component that can occur when using only a single age tracer (Bethke & Johnson, 2008). For each individual tracer (^{39}Ar , ^{14}C , $^4\text{He}_{\text{rad}}$) and mean age, significant linear correlations ($P < 0.05$) are observed between distance and increasing age (Figures 4a–4d), showing that groundwater

Table 6*Noble Gas Isotope Measurements, Reported as Replicate-Mean Delta Values With Respect to Atmospheric Air From Two Labs (Scripps Institution of Oceanography [SIO] and Woods Hole Oceanographic Institution's [WHOI])*

Lab:	$\delta^*\text{Kr}$	$\delta^*\text{Kr}$	$\delta^*\text{Xe}$	$\delta^*\text{Xe}$	$\Delta^{40}\text{Ar}$	$\Delta^{40}\text{Ar}$
	SIO	WHOI	SIO	WHOI	SIO	WHOI
Units:	per meg/amu	per meg/amu	per meg/amu	per meg/amu	per mil	per mil
G-006A	89	85	63	60	0.00	0.02
F-008A	89	89	62	66	0.03	0.05
E-014A	122	114	83	85	0.00	0.04
D-023A	180	162	172	144	0.00	0.03
D-016B	178	169	104	145	0.02	0.01
D-001A	132	120	81	81	−0.01	0.01
C-016B	115	102	81	76	0.02	0.05
B-110A	90	76	37	41	0.02	0.06
B-013B	142	139	83	97	−0.01	0.05
Martin	130	120	97	85	0.01	0.03

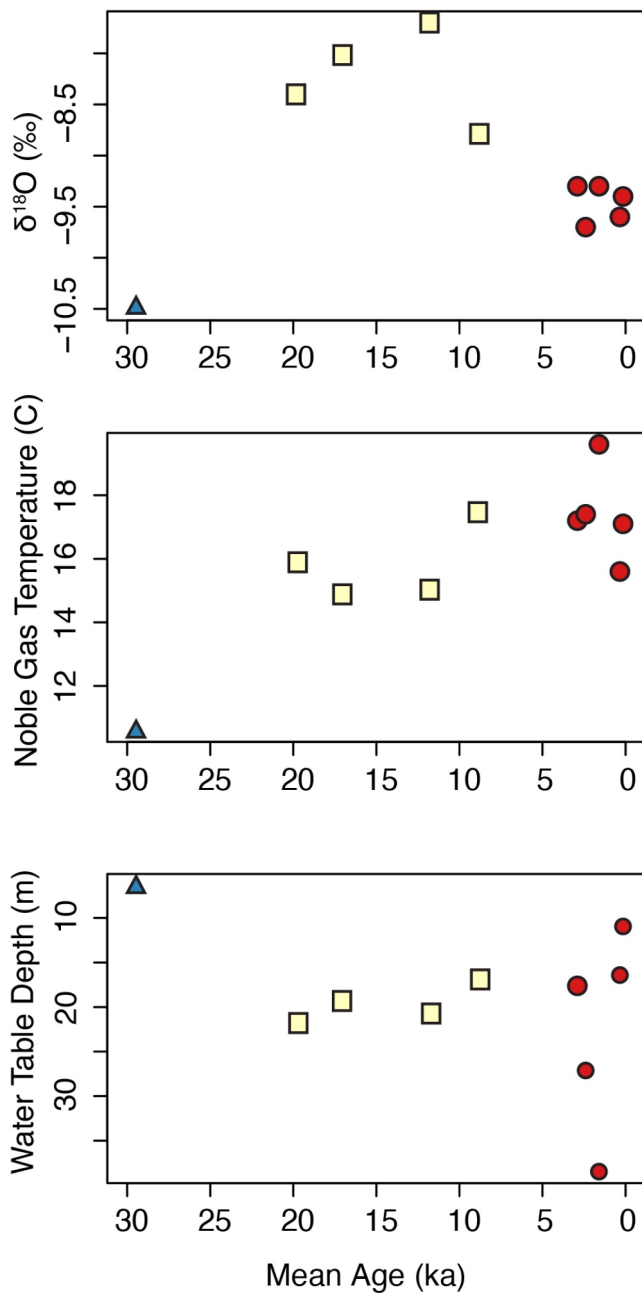


Figure 5. From top to bottom: plots of (a) $\delta^{18}\text{O}$ (‰ VSMOW), (b) noble gas temperature ($^{\circ}\text{C}$), and (c) water table depth (m) versus mean groundwater age (ka). Symbology of wells corresponds to three groups in Figure 3.

age is a function of position within the flow system. Radiogenic ^{40}Ar excess ($\Delta^{40}\text{Ar}$; Seltzer, Krantz, et al., 2021) was notably small in all wells (Table 6), on the order of the measurement precision (~ 0.02 per mil), but it was highest in well B-110-A (~ 0.06), consistent with the low ^{14}C and high $^4\text{He}_{\text{rad}}$ also observed in this well.

Groundwater sampled from B-110A appears to be an outlier, in that it lacks contributions from Holocene recharge. In addition to markedly older individual tracer and mean ages, groundwater from this well had the most positive $\delta^{13}\text{C}$ -DIC value, major ion chemistry indicative of cation exchange, the most negative $\delta^{18}\text{O}$ value, and noble gas concentrations suggestive of higher elevation and/or colder, more winter-dominated recharge (Eastoe & Towne, 2018). Compared to other wells, the geochemical and isotopic signature of this well may suggest that it is influenced by deeply circulated mountain-block recharge that has discharged into the basin aquifer system through a fault, as has been hypothesized in other parts of the Tucson Basin (Eastoe & Wright, 2019; Eastoe et al., 2004; Markovich et al., 2021). This may also be in part due to a deeper well screen interval, essentially eliminating contributions of Holocene-aged groundwater mixing at the well.

5.2. Sample Groups and Paleoclimate

Integrating the various geochemical, isotopic, and noble gas tracers, three groupings of samples along the transect representing distinct hydroclimatic time periods in the basin from the LGM to present (Figures 3, 4a–4d, and 5a–5c) were observed. Group 1 includes the first five wells along the transect, which exhibit late Holocene mean ages (~ 2.9 – 0.15 ka) and $\delta^{18}\text{O}$ values ranging from -9.7 to -9.3 ‰, generally plotting below the modern LMWL, but along the GMWL, and between modern winter and summer precipitation values (Figure 3; Eastoe & Wright, 2019). NGTs ranged between 15.6 and 19.6°C during this time and estimated WTDs were between 38.47 and 22.06 m, with the lowest WTD occurring between 2.9 and 1.6 ka. This stark decline in the water table during the mid- to late-Holocene coincides with the warmest NGT and suggests this may have been a period of maximum aridity in the Tucson Basin.

Group 2 includes the subsequent four wells along the transect (excluding B-110A), with LGM to early Holocene mean ages ranging from ~ 19.8 to 8.8 ka. $\delta^{18}\text{O}$ values span a somewhat larger range from -8.8 to -7.7 ‰ with all samples plotting below the GMWL, but slightly more positive than Group 1 samples, clustering around modern summer precipitation values (Figure 3; Eastoe & Wright, 2019). NGTs were between 14.9 and 17.5°C and WTDs ranged from 17.02 to 21.89 m during this time. Observed NGTs and WTDs are consistent with previous evidence for an LGM hydroclimate in the southwestern U.S. that was cooler with net higher recharge rates (e.g., Kaufman et al., 2020; Phillips et al., 1986; Seltzer, Ng, et al., 2021; Zhu et al., 1998). $\delta^{18}\text{O}$ values of recharge have been shown to be more negative

during the LGM in many regions, including the southwest U.S. (e.g., Jasechko, 2016). However, the opposite is observed in the present study with LGM recharge having more positive $\delta^{18}\text{O}$ (similar to modern summer precipitation (monsoon) values; Figure 3; Eastoe & Wright, 2019) than late Holocene waters. We hypothesize that the $\delta^{18}\text{O}$ pattern in the Tucson Basin is related to a shift in the seasonality of recharge (e.g., Eastoe, 2023; Eastoe & Towne, 2018; Eastoe & Wright, 2019). Late Pleistocene to early Holocene groundwater may have had a higher proportion of summer monsoonal recharge, while late Holocene samples carry a signature more representative of today's climatic conditions dominated by relatively low $\delta^{18}\text{O}$ mountain front recharge consisting of 50 – 90% winter precipitation (Figure 3; Eastoe & Wright, 2019).

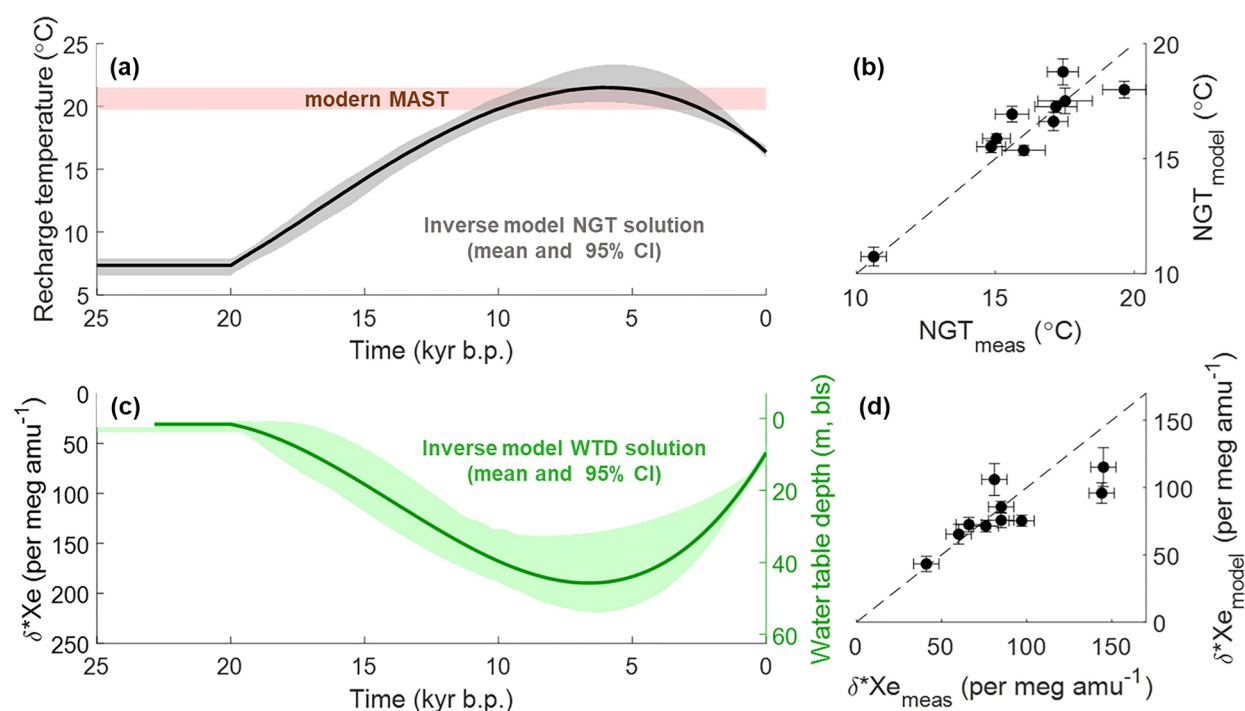


Figure 6. Plots showing (a) Reconstruction of recharge temperature ($^{\circ}\text{C}$) over time (thousands of years before present, kyr b.p.) in relation to modern mean annual surface temperature, (b) goodness of fit of modeled versus measured noble gas temperatures ($^{\circ}\text{C}$), (c) measured $\delta^*\text{Xe}$ (per meg amu^{-1}) and reconstruction of water table depths (m, bls) over time (kyr b.p.), and (d) goodness of fit of modeled versus measured $\delta^*\text{Xe}$ (per meg amu^{-1}).

Group 3 includes B-110A, which has the oldest mean age of 29.5 ka, the highest $^4\text{He}_{\text{rad}}$ abundance, the most negative $\delta^{18}\text{O}$ value (-10.5‰), and a lower-than-predicted δD value (-79.5‰) compared to the LMWL, GMWL, and modern winter precipitation (Figure 3; Eastoe & Wright, 2019). These low δD and $\delta^{18}\text{O}$ values are consistent with other values of late Pleistocene groundwater in southeastern Arizona (Eastoe & Wright, 2019), plotting well below both the LMWL and GMWL. Group 3 has an NGT substantially cooler than all other samples at 10.6°C , suggesting that this sample is uniquely isolated from modern recharge, with a negligible contribution from Holocene-aged waters to its residence time distribution function. Finally, the markedly shallower reconstructed WTD of 6.35 m suggests that net groundwater recharge rates were likely greater during the LGM than the mid-Holocene, consistent with noble gas constraints on past water table fluctuations in southern California (Seltzer, Ng, Danskin, et al., 2019).

Notably, even without consideration of mixing (i.e., via the inverse model framework in this study), the $\sim 9^{\circ}\text{C}$ range we find in apparent recharge temperature (i.e., NGT) far exceeds the $5\text{--}7^{\circ}\text{C}$ LGM-Holocene difference seen in other noble gas records from the U.S. southwest (Kulongoski et al., 2009; Seltzer, Krantz, et al., 2021; Seltzer, Ng, et al., 2021; Stute et al., 1992). When applying the inverse model to disentangle the effects of mixing, the range in recharge temperature is expanded to nearly 15°C (Figure 6a). We suggest that NGTs are suppressed below MAST in the LGM and late Holocene by cold mountain front recharge, as was shown by a recent study focused on recharge in the nearby Santa Catalina mountains (Markovich et al., 2021) and elsewhere in the southwestern U.S. (e.g., Manning, 2011). Field studies in the region have demonstrated that infiltration of water into washes following storm events can result in groundwater recharge a few degrees colder than mean annual surface air temperatures (Constantz et al., 2001). Estimates of Péclet number suggest that infiltration rates observed beneath washes in the Tucson region are sufficiently high to allow for advection-dominated heat transport following storm events or snow melt (See Appendix C in Supporting Information S1). This hypothesis is strongly supported by noble gas isotope-based WTD information, which shows a substantial deepening of the recharge-area water table during the mid-Holocene coincident with the warmest noble gas-based recharge temperatures, while colder-than-MAST NGTs in the late Holocene are associated with a shallower water table. To the extent that recharge intensity exerts a primary control on WTD, these findings suggest that the rate of recharge was higher in the LGM (and is higher today) than during the mid-Holocene, allowing cold mountain front

recharge to rapidly infiltrate the subsurface and thereby suppressing water table temperature in the recharge area below MAST. Measurements of colder-than-MAST groundwater at the most upgradient well during sampling support this notion. During the mid-Holocene, we hypothesize that a pronounced reduction in recharge greatly reduced the advection of cold mountain front recharge to the water table, reducing or eliminating the suppression of water table temperature and resulting in an apparent recharge temperature close to modern MAST. Thus, our findings point to (a) a reduction in recharge temperature in the LGM that was driven both by climatic cooling and by enhanced MFR, and (b) a dry mid-Holocene with a MAST that was likely close to modern MAST.

5.3. Evaluation of the Tracer Inverse Model Approach

To evaluate the inverse modeling approach, we convolve the LPM-based residence time distributions from each well with the inverse-model histories of NGT and δ^*Xe to compute “predicted” NGT and δ^*Xe values that we expect to observe at each well, due to mixing of different-aged waters. In other words, this evaluation compares measured NGT and δ^*Xe with modeled NGT and δ^*Xe , where modeled values are computed via Equations 4 and 5. For clarity, modeled NGT and δ^*Xe are distinct for each well, but the reconstructed time histories of NGT and δ^*Xe (used in Equations 4 and 5) are shared by all wells. Figures 6b and 6d show this goodness-of-fit evaluation by comparing measured and modeled NGT and δ^*Xe across all wells in the study. We find a root-mean-square-deviation (measured vs. modeled) of 0.9°C for NGT and 21.5 per meg amu^{-1} for δ^*Xe (equivalent to ~ 5 m WTD).

While this goodness-of-fit evaluation provides some confidence in the inverse model-based reconstructions of temperature and WTD, we note that a major limitation of this approach is that there is no explicit consideration of age uncertainties. The novelty of this approach—and its utility for wells displaying substantial mixing of different-aged waters—is that it treats geochemical measurements in a well as reflecting a distribution of waters recharged at different times, rather than a single point in time. However, a drawback of this approach is that systematic uncertainties in the age distribution—resulting from the choice of lumped parameter model or the geochemical tracer model (e.g., uncertainties in the radiocarbon correction model)—are not explicitly accounted for, unlike uncertainties in the recharge parameters (NGT and δ^*Xe), which are captured by the monte carlo approach. Consequently, the findings may not be unique, as there may be other combinations of residence time distribution functions that may in principle satisfy the constraints of the inverse model. The close agreement of measured and model parameter values (Figure 6) and the compatibility of the temperature and WTD time histories with the consensus view of regional paleoclimate (Section 5.4) both provide confidence in the inverse model solutions found in this study. Nonetheless, the potential for non-uniqueness is a limitation that should be noted.

5.4. Comparison With Other Paleoclimate Proxies

Multiple lines of paleoclimate evidence suggest a peak in aridity in much of the southwest U.S. ~ 6 ka (Thompson et al., 1993), including LS (Castiglia & Fawcett, 2006; Waters, 1989), packrat middens (Holmgren et al., 2006; Van Devender & Spaulding, 1979), speleothems (Wagner, 2006), which is consistent with our groundwater age distributions and noble gas constraints on temperature and WTD (Figures 5b, 5c, 6a, 6c, and 7). ^{14}C dating of LS from Lake Cochise (Waters, 1989) ~ 78 km east of the study area reveals a lacustral event at/before ~ 8.9 ka with an unknown period of desiccation to ~ 5.4 ka when another lacustral event may have occurred, as well as a lacustral event ~ 4 – 3 ka. LS from northern Mexico (Castiglia & Fawcett, 2006) ~ 320 km southeast of the study area generally agree with the observations from Waters (1989), with the existence of pluvial lakes 8.5–8.3, 6.7–6.1, 4.3–3.8, and 0.22 ka. Additionally, reconstructed Colorado River flows at Lees Ferry, Arizona using tree ring data (Meko et al., 2007) reveal several multi-decade periods of reduced flow ~ 1.2 – 0.02 ka. Comparing the two youngest groundwater samples in the Tucson Basin, with mean ages of 0.34 and 0.15 ka, reveals that they generally coincide with periods of increasing or above average flow in the Colorado River (Meko et al., 2007). That said, inferences from other paleoclimate proxies are often at odds with one another in delineating cooler/warmer or drier/wetter periods.

It is also important to consider that different paleoclimate proxies have varying limitations and uncertainties. For example, while packrat middens have been the mainstay for paleoclimate interpretations in the semi-arid southwest, a well-documented absence in the mid-Holocene limits their usefulness to ~ 9 – 4 ka (Betancourt et al., 1993). Additionally, based on the vast amount of paleoclimate data that exists for the southwest U.S., it is apparent that climatic conditions are highly regionally variable. The current study shows that multiple

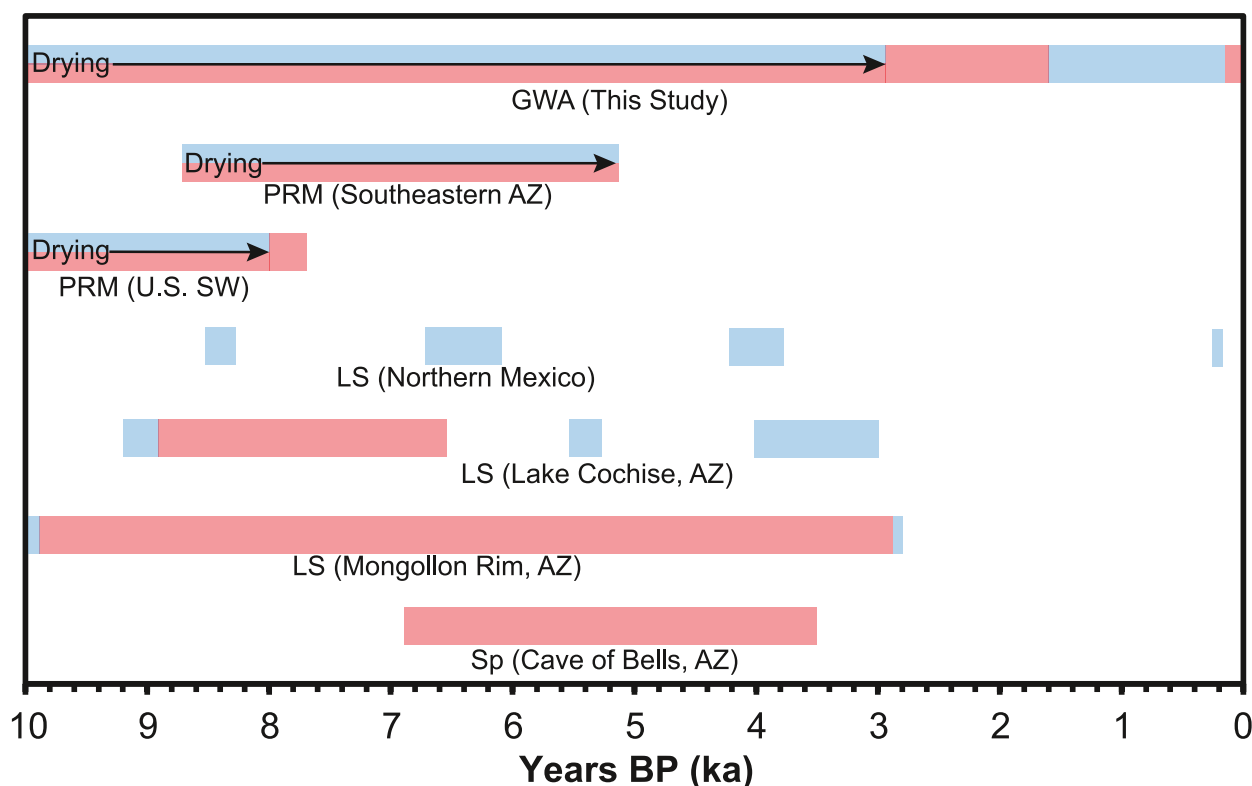


Figure 7. Interpretations of warmer/drier (red boxes) or cooler/wetter (blue boxes) climates by groundwater age distributions (GWA; this study) and other paleoclimate proxies including speleothems (Sp; Wagner, 2006), lacustrine sediments (LS; Allen & Anderson, 1993; Castiglia & Fawcett, 2006; Waters, 1989), and packrat middens (PRM; Holmgren et al., 2006; Van Devender & Spaulding, 1979) in thousand years (ka) before present (BP). Overlapping red and blue boxes for the same time period indicates there is inconclusive or diverging evidence of both warmer/drier and cooler/wetter conditions in the same study areas based on interpretations from multiple paleoclimate indicators with differing sensitivities to climate perturbations.

groundwater age tracers of varying timescales in conjunction with traditional noble gas data (NGTs) and more novel noble gas stable isotope data (WTDs) can be used concurrently to infer changes in groundwater systems over time. This information is valuable in filling in knowledge gaps or uncertainties about paleoclimate across the mid- to late-Holocene left by other proxies.

5.5. Implications for Groundwater Resource Management

The spectrum of groundwater ages from Pleistocene to modern, coinciding with current hydraulic gradients, indicates that recharge has been relatively continuous for the last several thousand years in the Tucson Basin. Although groundwater levels (related to recharge rates) have varied over time, there is little evidence for a complete hiatus in recharge, even during the mid-Holocene arid period. Current recharge rates have been high enough to increase WTDs by ~27.5 m since the mid-Holocene, increasing the amount of water in storage over the past few millennia.

These fluctuations in WTDs over the past ~16.5 ka (~32 m) are only half of the amount of water level decreases observed in the Tucson Basin due to groundwater abstraction over the past ~70 years (Tillman & Flynn, 2023). Given the high rates of groundwater extraction in parts of the Tucson Basin today, depletion due to pumping would likely be occurring under any of the hydroclimatic conditions present since the LGM (e.g., even during the wettest periods on record). A similar situation has been observed in the Nubian aquifer, where changes in water levels from groundwater extraction over the last several decades (Mohamed Ibrahim, 2019; Voss & Soliman, 2014) exceed the difference between water levels associated with wetter conditions at ~320 ka and the late Holocene (Ram et al., 2022). Given the long timescales for regional aquifer systems to respond to shifts in climate (e.g., Rousseau-Gueutin et al., 2013), groundwater extraction rather than climate should be expected to be the

main driver of changes in groundwater storage in the Tucson Basin—and likely other arid to semi-arid regions—over the coming decades.

The presence of modern recharge suggests that there is a pathway to sustainable development of groundwater resources in the Tucson area. Recharge rates should not typically be used to determine sustainable groundwater extraction, because extracted volumes are typically balanced by capture of groundwater discharge and depletion of storage (Bredehoeft, 2002; Konikow & Leake, 2014). However, where substantial depletion has already occurred and discharge of groundwater to surface water bodies no longer occurs, drawdown will stabilize when it is balanced by recharge (Butler et al., 2023).

6. Summary and Conclusions

This study combined conventional and more novel groundwater age tracers, including ^3H , ^{85}Kr , ^{39}Ar , ^{14}C , and ^4He , to span the full range of groundwater age distributions and constrain mean ages along a well-defined groundwater flow path in the Tucson Basin. Noble gases were used to determine temperatures and WTD at the time and place of recharge. Results were integrated with inverse modeling to examine whether changes in climate are recorded in groundwater age distributions present in the basin, and whether these signals align with paleoclimate inferences made using other types of proxies (e.g., packrat middens, LS).

Mean groundwater ages, NGTs, WTDs, and $\delta^{18}\text{O}$ show a substantial change in climate from the late Pleistocene through Holocene. The LGM age groundwater samples show colder recharge temperatures and shallower water tables—likely indicating higher net recharge rates—compared to the early-Holocene. Climate was somewhat consistent from the early- to mid-Holocene with little variation in NGT, WTD, and $\delta^{18}\text{O}$. However, there was an abrupt increase in NGTs and WTDs during the mid- to late-Holocene, signifying a period of maximum aridity and substantially reduced recharge rates. These results provide new independent evidence supporting a dry and warm mid-Holocene in the southwestern United States. The warming trend in recharge temperatures from the late Pleistocene through Holocene reflects both a climatic warming and greater suppression of water table temperature by enhanced mountain front recharge. Finally, a shift in $\delta^{18}\text{O}$ toward more positive values in the mid Holocene, relative to the LGM and late Holocene, may reflect a change in the seasonality of recharge from more summer- to winter-dominated, suggesting that enhanced aridity in the mid Holocene may be attributable primarily to a reduction of wintertime precipitation from westerly Pacific storms.

The groundwater age distributions, spanning centennial to millennial timescales, across the Tucson Basin, suggest that while climate has changed considerably since the late Pleistocene, recharge to the basin has been somewhat continuous, despite a likely reduction in the mid-Holocene. Discordant tracer ages derived from ^3H , ^{85}Kr , ^{39}Ar , ^{14}C , and/or $^4\text{He}_{\text{rad}}$ suggest the presence of “young” and “old” groundwater components likely due to varying groundwater flow paths and long screened production wells in an active regional groundwater flow system. Measurement of ^{39}Ar was particularly useful in detecting “intermediate age” groundwater. The presence of fossil groundwater in the Tucson Basin is attributed to the long transport distances from the area of mountain front recharge and lack of diffuse basin recharge. The decline in the regional water table resulting from the extraction of groundwater over the last approximately 70 years exceeds the natural fluctuations over the past approximately 30 ka. This illustrates that human influence not only prevails in shaping climate change but also significantly impacts the subsurface water cycle. The occurrence of recharge over long time periods is critical information for water resources managers in the Tucson Basin and likely for other aquifer systems in the southwestern U.S. and other semi-arid regions that contain fossil groundwater that are undergoing depletion.

Data Availability Statement

All chemical, isotopic, and noble gas data generated in this study are included in tables in the main document. The data has also been uploaded to CUAHSI Hydroshare and is available online at (McIntosh et al., 2025).

References

- Aeschbach-Hertig, W., Peeters, F., Beyerle, U., & Kipfer, R. (2000). Palaeotemperature reconstruction from noble gases in ground water taking into account equilibration with entrapped air. *Nature*, 405(6790), 1040–1044. <https://doi.org/10.1038/35016542>
- Aeschbach-Hertig, W., & Solomon, D. K. (2013). Noble gas thermometry in groundwater hydrology. In *Advances in isotope geochemistry*. https://doi.org/10.1007/978-3-642-28836-4_5

Acknowledgments

This work was supported in part by research grants from the United States Geological Survey, the Natural Sciences and Engineering Research Council of Canada, the University of Arizona Graduate & Professional Student Council, and the Geological Society of America. The contributions of K.C. Carroll were supported by the Department of Energy Environmental Management Minority Serving Institution Partnership Program (EM-MSIPP) managed by the Savannah River National Laboratory. A.M. Seltzer was supported by NSF EAR-2102457. J.C. McIntosh was supported by the Thomas Meixner Endowed Chair, Department of Hydrology & Atmospheric Sciences, University of Arizona, and CIFAR Earth4D Subsurface Science & Exploration Program (McIntosh is a fellow). Gratitude is expressed to Tucson Water for providing access to their wells, especially Dick Thompson, Margaret Snyder, and Michael Liberti, who provided extensive logistical, field, and water table elevations mapping support.

- Ajami, H., Troch, P. A., Maddock III, T., Meixner, T., & Eastoe, C. (2011). Quantifying mountain block recharge by means of catchment-scale storage-discharge relationships. *Water Resources Research*, 47(4), W04504. <https://doi.org/10.1029/2010wr009598>
- Allen, B. D., & Anderson, R. Y. (1993). Evidence from western North America for rapid shifts in climate during the last glacial maximum. *Science*, 260(5116), 1920–1923. <https://doi.org/10.1126/science.260.5116.1920>
- Appelo, C. A. J. (1994). Cation and proton exchange, pH variations, and carbonate reactions in a freshening aquifer. *Water Resources Research*, 30(10), 2793–2805. <https://doi.org/10.1029/94wr01048>
- Ballentine, C. J., & Burnard, P. G. (2002). Production, release and transport of noble gases in the Continental crust. *Reviews in Mineralogy and Geochemistry*, 47(1), 481–538. <https://doi.org/10.2138/rmg.2002.47.12>
- Ballentine, C. J., O'Nions, R. K., & Coleman, M. L. (1996). A Magnus opus: Helium, neon, and argon isotopes in a North Sea oilfield. *Geochimica et Cosmochimica Acta*, 60(5), 831–849. [https://doi.org/10.1016/0016-7037\(95\)00439-4](https://doi.org/10.1016/0016-7037(95)00439-4)
- Betancourt, J. L., Pierson, E. A., Rylander, K. A., Fairchild-Parks, J. A., & Dean, J. S. (1993). Influence of history and climate on New Mexico pinon-juniper woodlands. In *USDA Forest service general technical report RM-236* (pp. 42–62).
- Bethke, C. M., & Johnson, T. M. (2008). Groundwater age and groundwater age dating. *Annual Review of Earth and Planetary Sciences*, 36(1), 121–152. <https://doi.org/10.1146/annurev.earth.36.031207.124210>
- Bierkens, M. F. P., & Wada, Y. (2019). Non-renewable groundwater use and groundwater depletion: A review. *Environmental Research Letters*, 14(6), 063002. <https://doi.org/10.1088/1748-9326/ab1a5f>
- Bredehoeft, J. D. (2002). The water budget myth revisited: Why hydrogeologists model. *Groundwater Series*, 40(4), 340–345. <https://doi.org/10.1111/j.1745-6584.2002.tb02511.x>
- Bromwich, D. H., Toracinta, E. R., Wei, H., Oglesby, R. J., Fastook, J. L., & Hughes, T. J. (2004). Polar MM5 simulations of the Winter climate of the Laurentide ice sheet at the LGM. *Journal of Climate*, 17(17), 3415–3433. [https://doi.org/10.1175/1520-0442\(2004\)017<3415:PMSOTW>2.0.CO;2](https://doi.org/10.1175/1520-0442(2004)017<3415:PMSOTW>2.0.CO;2)
- Butler, J. J., Jr., Bohling, G. C., Perkins, S. P., Whittemore, D. O., Liu, G., & Wilson, B. B. (2023). Net inflow: An important target on the path to aquifer sustainability. *Groundwater Series*, 61(1), 56–65. <https://doi.org/10.1111/gwat.13233>
- Castiglia, P. J., & Fawcett, P. J. (2006). Large Holocene lakes and climate change in the Chihuahuan Desert. *Geology*, 34(2), 113. <https://doi.org/10.1130/G22036.1>
- Castro, M. C., Stute, M., & Schlosser, P. (2000). Comparison of 4He ages and 14C ages in simple aquifer systems: Implications for groundwater flow and chronologies. *Applied Geochemistry*, 15(8), 1137–1167. [https://doi.org/10.1016/S0883-2927\(99\)00113-4](https://doi.org/10.1016/S0883-2927(99)00113-4)
- Clark, I. D., & Fritz, P. (1997). *Environmental isotopes in hydrogeology*. CRC Press.
- COHMAP, M. (1988). Climatic changes of the last 18,000 years: Observations and model simulations. *Science*, 241(4869), 1043–1052. <https://doi.org/10.1126/science.241.4869.1043>
- Constantz, J., Stonestrom, D., Stewart, A. E., Niswonger, R., & Smith, T. R. (2001). Analysis of streambed temperatures in ephemeral channels to determine streamflow frequency and duration. *Water Resources Research*, 37(2), 317–328. <https://doi.org/10.1029/2000wr900271>
- Craig, H. (1961). Isotopic variations in meteoric waters. *Science*, 133(3465), 1702–1703. <https://doi.org/10.1126/science.133.3465.1702>
- Craig, H., & Lupton, J. E. (1976). Primordial neon, helium, and hydrogen in oceanic basalts. *Earth and Planetary Science Letters*, 31(3), 369–385. [https://doi.org/10.1016/0012-821X\(76\)90118-7](https://doi.org/10.1016/0012-821X(76)90118-7)
- Cuthbert, M. O., Gleeson, T., Bierkens, M. F. P., Ferguson, G., & Taylor, R. G. (2023). Defining renewable groundwater use and its relevance to sustainable groundwater management. *Water Resources Research*, 59(9), e2022WR032831. <https://doi.org/10.1029/2022wr032831>
- Cuthbert, M. O., Gleeson, T., Moosdorf, N., Befus, K. M., Schneider, A., Hartmann, J., & Lehner, B. (2019). Global patterns and dynamics of climate-groundwater interactions. *Nature Climate Change*, 9(2), 137–141. <https://doi.org/10.1038/s41558-018-0386-4>
- Davidson, E. S. (1973). Geohydrology and water resources of the Tucson Basin, Arizona. In *U.S. geological Survey, water-supply paper 1939-E*.
- Eastoe, C. J. (2023). Isotope record of groundwater recharge mechanisms and climate change in southwestern North America. *Applied Geochemistry*, 151, 105604. <https://doi.org/10.1016/j.apgeochem.2023.105604>
- Eastoe, C. J., & Dettman, D. L. (2016). Isotope amount effects in hydrologic and climate reconstructions of monsoon climates: Implications of some long-term data sets for precipitation. *Chemical Geology*, 430, 78–89. <https://doi.org/10.1016/j.chemgeo.2016.03.022>
- Eastoe, C. J., Gu, A., & Long, A. (2004). The origins, ages and flow paths of groundwater in Tucson Basin: Results of a Study of multiple isotope systems. In *Groundwater recharge in a desert environment: The Southwestern United States* (Vol. 9, pp. 217–234). <https://doi.org/10.1029/009WSA12>
- Eastoe, C. J., & Towne, D. (2018). Regional zonation of groundwater recharge mechanisms in alluvial basins of Arizona: Interpretation of isotope mapping. *Journal of Geochemical Exploration*, 194, 134–145. <https://doi.org/10.1016/j.gexplo.2018.07.013>
- Eastoe, C. J., & Wright, W. E. (2019). Hydrology of mountain blocks in Arizona and New Mexico as revealed by isotopes in groundwater and precipitation. *Geosciences*, 9(11), 461. <https://doi.org/10.3390/geosciences9110461>
- Faulstich, H. L., Woodhouse, C. A., & Griffin, D. (2012). Reconstructed cool- and warm-season precipitation over the tribal lands of northeastern Arizona. *Climatic Change*, 118(2), 457–468. <https://doi.org/10.1007/s10584-012-0626-y>
- Ferguson, G., Cuthbert, M. O., Befus, K., Gleeson, T., & McIntosh, J. C. (2020). Rethinking groundwater age. *Nature Geoscience*, 13(9), 592–594. <https://doi.org/10.1038/s41561-020-0629-7>
- Gieskes, J. M., & Rogers, W. C. (1973). Alkalinity determination in interstitial waters of marine sediments. *Journal of Sedimentary Research*, 43(1), 272–277. <https://doi.org/10.1306/74D72743-2B21-11D7-8648000102C1865D>
- Glueck, J. R. (1997). Climate of Tucson. In *U.S. Department of Commerce, NOAA technical memorandum NWS WR-249*.
- Hanson, R. T., Anderson, S. R., & Pool, D. R. (1990). *Simulation of ground-water flow and potential land subsidence, Avra Valley, Arizona* (Vol. 90, p. 4178). US Department of the Interior, US Geological Survey.
- Hanson, R. T., & Benedict, J. F. (1994). *Simulation of ground-water flow and potential land subsidence, upper Santa Cruz Basin, Arizona* (Vol. 93, p. 4196). US Department of the Interior, US Geological Survey.
- Hersbach, H., Bell, B., Berrisford, P., Hirahara, S., Horányi, A., Muñoz-Sabater, J., et al. (2020). The ERA5 global reanalysis. *Quarterly Journal of the Royal Meteorological Society*, 146(730), 1999–2049. <https://doi.org/10.1002/qj.3803>
- Hilton, D. R. (1996). The helium and carbon isotope systematics of a continental geothermal system: Results from monitoring studies at Long Valley caldera (California, USA). *Chemical Geology*, 127(4), 269–295. [https://doi.org/10.1016/0009-2541\(95\)00134-4](https://doi.org/10.1016/0009-2541(95)00134-4)
- Holmgren, C. A., Betancourt, J. L., & Rylander, K. A. (2006). A 36,000-yr vegetation history from the Peloncillo Mountains, southeastern Arizona, USA. *Palaeogeography, Palaeoclimatology, Palaeoecology*, 240(3–4), 405–422. <https://doi.org/10.1016/j.palaeo.2006.02.017>
- Hopkins, C. B., McIntosh, J. C., Eastoe, C., Dickinson, J. E., & Meixner, T. (2014). Evaluation of the importance of clay confining units on groundwater flow in alluvial basins using solute and isotope tracers: The case of Middle San Pedro Basin in southeastern Arizona (USA). *Hydrogeology Journal*, 22(4), 829–849. <https://doi.org/10.1007/s10040-013-1090-0>

- Jasechko, S. (2016). Partitioning young and old groundwater with geochemical tracers. *Chemical Geology*, 427, 35–42. <https://doi.org/10.1016/j.chemgeo.2016.02.012>
- Jasechko, S., Perrone, D., Befus, K. M., Bayani Cardenas, M., Ferguson, G., Gleeson, T., et al. (2017). Global aquifers dominated by fossil groundwaters but wells vulnerable to modern contamination. *Nature Geoscience*, 10(6), 425–429. <https://doi.org/10.1038/ngeo2943>
- Jung, M., & Aeschbach, W. (2018). A new software tool for the analysis of noble gas data sets from (ground)water. *Environmental Modelling & Software*, 103, 120–130. <https://doi.org/10.1016/j.envsoft.2018.02.004>
- Jung, M., Wieser, M., von Oehsen, A., & Aeschbach-Hertig, W. (2013). Properties of the closed-system equilibration model for dissolved noble gases in groundwater. *Chemical Geology*, 339, 291–300. <https://doi.org/10.1016/j.chemgeo.2012.08.006>
- Jurgens, B. C., Bohle, J. K., & Eberts, S. M. (2012). TracerLPM (Version 1): An Excel® workbook for interpreting groundwater age distributions from environmental tracer data. In *United States geological Survey, techniques and methods report 4-F3* (p. 60). United States Geological Survey.
- Kalin, R. M. (1994). *Using isotopes and solute tracers to infer groundwater recharge and flow in the Cienega Creek Watershed, SE Arizona*. Ph. D. Dissertation. Department of Hydrology and Water Resources, University of Arizona.
- Kaufman, D., McKay, N., Routson, C., Erb, M., Davis, B., Heiri, O., et al. (2020). A global database of Holocene paleotemperature records. *Scientific Data*, 7(1), 115. <https://doi.org/10.1038/s41597-020-0445-3>
- Kipfer, R., Aeschbach-Hertig, W., Peeters, F., & Stute, M. (2002). Noble gases in lakes and ground waters. *Reviews in Mineralogy and Geochemistry*, 47(1), 615–700. <https://doi.org/10.2138/rmg.2002.47.14>
- Konikow, L. F., & Leake, S. A. (2014). Depletion and capture: Revisiting “the source of water derived from wells”. *Groundwater Series*, 52(S1), 100–111. <https://doi.org/10.1111/gwat.12204>
- Krider, P. R. (1997). Paleoclimatic significance of late Quaternary Lacustrine and alluvial stratigraphy, Animas Valley, New Mexico. *Quaternary Research*, 50(3), 283–289. <https://doi.org/10.1006/qres.1998.1997>
- Kulogowski, J. T., Hilton, D. R., Izbicki, J. A., & Belitz, K. (2009). Evidence for prolonged El Nino-like conditions in the Pacific during the Late Pleistocene: A 43 ka noble gas record from California groundwaters. *Quaternary Science Reviews*, 28(23), 2465–2473. <https://doi.org/10.1016/j.quascirev.2009.05.008>
- Laney, R. L. (1972). *Chemical quality of the water in the Tucson Basin, Arizona*. U.S. Geological Survey, Water-Supply Paper 1939-D.
- Liu, S., Jiang, D., & Lang, X. (2018). A multi-model analysis of moisture changes during the last glacial maximum. *Quaternary Science Reviews*, 191, 363–377. <https://doi.org/10.1016/j.quascirev.2018.05.029>
- Loosli, H. H. (1983). A dating method with ³⁹Ar. *Earth and Planetary Science Letters*, 63(1), 51–62. [https://doi.org/10.1016/0012-821X\(83\)90021-3](https://doi.org/10.1016/0012-821X(83)90021-3)
- Lora, J. M., Mitchell, J. L., & Tripathi, A. E. (2016). Abrupt reorganization of North Pacific and western North American climate during the last deglaciation. *Geophysical Research Letters*, 43(22), 11796–11804. <https://doi.org/10.1002/2016GL071244>
- Manning, A. H. (2011). Mountain-block recharge, present and past, in the eastern Española Basin, New Mexico, USA. *Hydrogeology Journal*, 19(2), 379–397. <https://doi.org/10.1007/s10040-010-0696-8>
- Margat, J., Foster, S., & Droubi, A. (2006). *Concept and Importance of non-renewable resources*. Non-Renewable Groundwater Resources.
- Markovich, K. H., Condon, L. E., Carroll, K. C., Purtschert, R., & McIntosh, J. C. (2021). A mountain-front recharge component characterization approach combining groundwater age distributions, noble gas thermometry, and fluid and energy transport modeling. *Water Resources Research*, 57(1), e2020WR027743. <https://doi.org/10.1029/2020WR027743>
- Markovich, K. H., Manning, A. H., Condon, L. E., & McIntosh, J. C. (2019). Mountain-block recharge: A review of current understanding. *Water Resources Research*, 55(11), 8278–8304. <https://doi.org/10.1029/2019WR025676>
- McCallum, J. L., Cook, P. G., Dogramaci, S., Purtschert, R., Simmons, C. T., & Burk, L. (2017). Identifying modern and historic recharge events from tracer-derived groundwater age distributions. *Water Resources Research*, 53(2), 1039–1056. <https://doi.org/10.1002/2016WR019839>
- McIntosh, J., Noyes, C., Ferguson, G., Seltzer, A., Ng, J., Purtschert, R., et al. (2025). *Chemical, isotopic, age tracer, and noble gas data for Tucson Basin groundwater*. HydroShare. Retrieved from <http://www.hydroshare.org/resource/6cad951e972b4d0a91ab05dc1a861ec9>
- McMahon, P. B., Plummer, L. N., Böhlke, J. K., Shapiro, S. D., & Hinkle, S. R. (2011). A comparison of recharge rates in aquifers of the United States based on groundwater-age data. *Hydrogeology Journal*, 19(4), 779–800. <https://doi.org/10.1007/s10040-011-0722-5>
- Meko, D. M., Woodhouse, C. A., Baisan, C. A., Knight, T., Lucas, J. J., Hughes, M. K., & Salzer, M. W. (2007). Medieval drought in the upper Colorado River Basin. *Geophysical Research Letters*, 34(10), L10705. <https://doi.org/10.1029/2007GL029988>
- Mohamed Ibrahim, S. M. (2019). Effects of groundwater over-pumping on the sustainability of the Nubian Sandstone Aquifer in East-Oweinat Area, Egypt. *NRIAG Journal of Astronomy and Geophysics*, 8(1), 117–130. <https://doi.org/10.1080/20909977.2019.1639110>
- Ng, J., Tyne, R., Seltzer, A., Noyes, C., McIntosh, J., & Severinghaus, J. (2023). A new large-volume equilibration method for high-precision measurements of dissolved noble gas stable isotopes. *Rapid Communications in Mass Spectrometry*, 37(7), e9471. <https://doi.org/10.1002/rcm.9471>
- Olson, M. C. (1982). *Mountain-front recharge to the Tucson basin from Tanque Verde Canyon, Arizona*. M.S. thesis. Department of Hydrology and Water Resources, University of Arizona.
- Osman, M. B., Tierney, J. E., Zhu, J., Tardif, R., Hakim, G. J., King, J., & Poulsen, C. J. (2021). Globally resolved surface temperatures since the last Glacial Maximum. *Nature*, 599(7884), 239–244. <https://doi.org/10.1038/s41586-021-03984-4>
- Oster, J. L., Ibarra, D. E., Winnick, M. J., & Maher, K. (2015). Steering of westerly storms over western North America at the last Glacial Maximum. *Nature Geoscience*, 8(3), 201–205. <https://doi.org/10.1038/ngeo2365>
- Parada, C. B., Long, A., & Davis, S. N. (1983). Stable-isotopic composition of soil carbon dioxide in the Tucson basin, Arizona, U.S.A. *Chemical Geology*, 41, 219–236. [https://doi.org/10.1016/S0009-2541\(83\)80020-5](https://doi.org/10.1016/S0009-2541(83)80020-5)
- Parkhurst, D. L., & Charlton, S. R. (2008). *NetpathXL, an Excel Interface to the Program NETPATH* (p. 11). US Department of the Interior, US Geological Survey.
- Phillips, F. M., Peeters, L. A., Tansey, M. K., & Davis, S. N. (1986). Paleoclimatic inferences from an isotopic investigation of groundwater in the central San Juan Basin, New Mexico. *Quaternary Research*, 26(2), 179–193. [https://doi.org/10.1016/0033-5894\(86\)90103-1](https://doi.org/10.1016/0033-5894(86)90103-1)
- Phillips, J. D., Duval, J. S., & Ambroziak, R. A. (1993). *National geophysical data grids; gamma-ray, gravity, magnetic, and topographic data for the conterminous United States (No. 9)*. US Geological Survey.
- Plummer, L. N., Prestemon, E. C., & Parkhurst, D. L. (1994). An interactive code (NETPATH) for modeling net geochemical reactions along a flow path, version 2.0. In *Water-Resources investigations report* (Vol. 94, p. 4169).
- Ram, R., Solomon, D. K., Yokochi, R., Burg, A., Purtschert, R., Seltzer, A. M., et al. (2022). Large-scale paleo water-table rise in a deep desert aquifer recorded by dissolved noble gases. *Journal of Hydrology*, 612, 128114. <https://doi.org/10.1016/j.jhydrol.2022.128114>

- Reed, J. C., & Bush, C. A. (2005). *Generalized geologic map of the United States, Puerto Rico, and the U.S. Virgin Islands*. U.S. Geological Survey. Retrieved from <http://pubs.usgs.gov/atlas/geologic/>
- Riedmann, R. A., & Purtschert, R. (2016). Separation of argon from environmental samples for Ar-37 and Ar-39 analyses. *Separation and Purification Technology*, 170, 217–223. <https://doi.org/10.1016/j.seppur.2016.06.017>
- Rousseau-Gueutin, P., Love, A. J., Vasseur, G., Robinson, N. I., Simmons, C. T., & de Marsily, G. (2013). Time to reach near-steady state in large aquifers. *Water Resources Research*, 49(10), 6893–6908. <https://doi.org/10.1002/wrcr.20534>
- Saar, M. O., Castro, M. C., Hall, C. M., Manga, M., & Rose, T. P. (2005). Quantifying magmatic, crustal, and atmospheric helium contributions to volcanic aquifers using all stable noble gases: Implications for magmatism and groundwater flow. *Geochemistry, Geophysics, Geosystems*, 6(3), Q03008. <https://doi.org/10.1029/2004GC000828>
- Salzer, M. W., & Kipfmüller, K. F. (2005). Reconstructed temperature and precipitation on a millennial timescale from tree-rings in the southern Colorado Plateau, U.S.A. *Climatic Change*, 70(3), 465–487. <https://doi.org/10.1007/s10584-005-5922-3>
- Scanlon, B. R., Keese, K. E., Flint, A. L., Flint, L. E., Gaye, C. B., Edmunds, W. M., & Simmers, I. (2006). Global synthesis of groundwater recharge in semiarid and arid regions. *Hydrological Processes*, 20(15), 3335–3370. <https://doi.org/10.1002/hyp.6335>
- Schulz, S., Walther, M., Michelsen, N., Rausch, R., Dirks, H., Al-Saud, M., et al. (2017). Improving large-scale groundwater models by considering fossil gradients. *Advances in Water Resources*, 103, 32–43. <https://doi.org/10.1016/j.advwatres.2017.02.010>
- Seltzer, A. M., & Bekaert, D. V. (2022). A unified method for measuring noble gas isotope ratios in air, water, and volcanic gases via dynamic mass spectrometry. *International Journal of Mass Spectrometry*, 478, 116873. <https://doi.org/10.1016/j.ijms.2022.116873>
- Seltzer, A. M., Krantz, J., Ng, J., Danskin, W., Bekaert, D., Barry, P., et al. (2021). The triple argon isotope composition of groundwater on ten-thousand-year timescales. *Chemical Geology*, 583, 120458. <https://doi.org/10.1016/j.chemgeo.2021.120458>
- Seltzer, A. M., Ng, J., Aeschbach, W., Kipfer, R., Kulongoski, J. T., Severinghaus, J. P., & Stute, M. (2021). Widespread six degrees celsius cooling on land during the last Glacial Maximum. *Nature*, 593(7858), 228–232. <https://doi.org/10.1038/s41586-021-03467-6>
- Seltzer, A. M., Ng, J., Danskin, W. R., Kulongoski, J. T., Gannon, R. S., Stute, M., & Severinghaus, J. P. (2019). Deglacial water-table decline in Southern California recorded by noble gas isotopes. *Nature Communications*, 10(1), 5739. <https://doi.org/10.1038/s41467-019-13693-2>
- Seltzer, A. M., Ng, J., & Severinghaus, J. P. (2019). Precise determination of Ar, Kr and Xe isotopic fractionation due to diffusion and dissolution in fresh water. *Earth and Planetary Science Letters*, 514, 156–165. <https://doi.org/10.1016/j.epsl.2019.03.008>
- Seltzer, A. M., Shackleton, S. A., & Bourq, I. C. (2023). Solubility equilibrium isotope effects of noble gases in water: Theory and observations. *The Journal of Physical Chemistry B*, 10(45), 9802–9812. <https://doi.org/10.1021/acs.jpcc.3c05651>
- Solomon, D. K. (2000). 4He in groundwater. In P. G. Cook & A. L. Herczeg (Eds.), *Environmental tracers in subsurface hydrology* (pp. 425–439). Springer US. https://doi.org/10.1007/978-1-4615-4557-6_14
- Spaulding, W. G., Leopold, E. B., & van Devender, T. R. (1983). Late Wisconsin paleoecology of the American Southwest. In *Late-quaternary environments of the United States* (Vol. 1).
- Steponaitis, E., Andrews, A., McGee, D., Quade, J., Hsieh, Y. T., Broecker, W. S., et al. (2015). Mid-Holocene drying of the U.S. Great Basin recorded in Nevada speleothems. *Quaternary Science Reviews*, 127, 174–185. <https://doi.org/10.1016/j.quascirev.2015.04.011>
- Sturchio, N. C., Du, X., Purtschert, R., Lehmann, B. E., Sultan, M., Patterson, L. J., et al. (2004). One million year old groundwater in the Sahara revealed by krypton-81 and chlorine-36. *Geophysical Research Letters*, 31(5), L05503. <https://doi.org/10.1029/2003gl019234>
- Stute, M., Schlosser, P., Clark, J. F., & Broecker, W. S. (1992). Paleotemperatures in the Southwestern United States derived from noble gases in ground water. *Science*, 256(5059), 1000–1003. <https://doi.org/10.1126/science.256.5059.1000>
- Suckow, A. (2014). The age of groundwater—Definitions, models and why we do not need this term. *Applied Geochemistry*, 50, 222–230. <https://doi.org/10.1016/j.apgeochem.2014.04.016>
- Theodorsson, P. (1996). *Measurement of weak radioactivity*. World Scientific.
- Thompson, R. S., Whitlock, C., Bartlein, P. J., Harrison, S. P., & Spaulding, W. G. (1993). Climatic changes in the western United States since 18,000 years ago. In H. E. Wright & K. Kutzbach (Eds.), *Global climate since the last glacial maximum* (pp. 468–513). University of Minnesota Press.
- Tierney, J. E., Zhu, J., King, J., Malevich, S. B., Hakim, G. J., & Poulsen, C. J. (2020). Glacial cooling and climate sensitivity revisited. *Nature*, 584(7822), 569–573. <https://doi.org/10.1038/s41586-020-2617-x>
- Tillman, F. D., & Flynn, M. E. (2023). Arizona Groundwater Explorer: Interactive maps for evaluating the historical and current groundwater conditions in wells in Arizona, USA. *Hydrogeology Journal*, 32(2), 1–17. <https://doi.org/10.1007/s10040-023-02748-w>
- Torgersen, T. (1980). Controls on pore-fluid concentration of 4He and 222Rn and the calculation of 4He/222Rn ages. *Journal of Geochemical Exploration*, 13(1), 57–75. [https://doi.org/10.1016/0375-6742\(80\)90021-7](https://doi.org/10.1016/0375-6742(80)90021-7)
- Torgersen, T., & Clarke, W. B. (1985). Helium accumulation in groundwater. I: An evaluation of sources and the continental flux of crustal 4He in the great Artesian Basin, Australia. *Geochimica et Cosmochimica Acta*, 49(5), 1211–1218. [https://doi.org/10.1016/0016-7037\(85\)90011-0](https://doi.org/10.1016/0016-7037(85)90011-0)
- Valentine-Darby, P., Baril, L., Struthers, K., Filippone, C., Swann, D., Mathis, A., & Chambers, N. (2017). *Saguaro national Park: Natural resource condition assessment*. U.S. National Park Service.
- Van Devender, T. R., & Spaulding, W. G. (1979). Development of vegetation and climate in the southwestern United States. *Science*, 204(4394), 701–710. <https://doi.org/10.1126/science.204.4394.701>
- Visser, A., Broers, H. P., Purtschert, R., Sültenfuß, J., & de Jonge, M. (2013). Groundwater age distributions at a public drinking water supply well field derived from multiple age tracers (85Kr, 3H/3He, and 39Ar). *Water Resources Research*, 49(11), 7778–7796. <https://doi.org/10.1002/2013WR014012>
- Voss, C. I., & Soliman, S. M. (2014). The transboundary non-renewable Nubian Aquifer System of Chad, Egypt, Libya and Sudan: Classical groundwater questions and parsimonious hydrogeologic analysis and modeling. *Hydrogeology Journal*, 22(2), 441–468. <https://doi.org/10.1007/s10040-013-1039-3>
- Wagner, J. D. M. (2006). *Speleothem record of southern Arizona paleoclimate, 54 to 2.5 ka. M.S. Thesis*. Department of Hydrology and Water Resources, University of Arizona.
- Waters, M. R. (1989). Late Quaternary lacustrine history and paleoclimatic significance of pluvial Lake Cochise, southeastern Arizona. *Quaternary Research*, 32(1), 1–11. [https://doi.org/10.1016/0033-5894\(89\)90027-6](https://doi.org/10.1016/0033-5894(89)90027-6)
- Weiss, R. F. (1968). Piggyback sampler for dissolved gas studies on sealed water samples. In *Deep sea research and oceanographic abstracts* (Vol. 15, pp. 695–699). Elsevier. [https://doi.org/10.1016/0011-7471\(68\)90082-x](https://doi.org/10.1016/0011-7471(68)90082-x)
- Wong, C. I., Banner, J. L., & Musgrove, M. L. (2015). Holocene climate variability in Texas, USA: An integration of existing paleoclimate data and modeling with a new, high-resolution speleothem record. *Quaternary Science Reviews*, 127, 155–173. <https://doi.org/10.1016/j.quascirev.2015.06.023>

- Woodhouse, C. A., Meko, D. M., Griffin, D., & Castro, C. L. (2013). Tree rings and multiseason drought variability in the lower Rio Grande Basin, USA. *Water Resources Research*, 49(2), 844–850. <https://doi.org/10.1002/wrcr.20098>
- Yokochi, R., Ram, R., Zappala, J. C., Jiang, W., Adar, E., Bernier, R., et al. (2019). Radiokrypton unveils dual moisture sources of a deep desert aquifer. *Proceedings of the National Academy of Sciences*, 116(33), 16222–16227. <https://doi.org/10.1073/pnas.1904260116>
- Zhu, C., Waddell, R. K., Star, I., & Ostrander, M. (1998). Responses of ground water in the Black Mesa basin, northeastern Arizona, to paleoclimatic changes during the late Pleistocene and Holocene. *Geology*, 26(2), 127. [https://doi.org/10.1130/0091-7613\(1998\)026<0127:ROGWIT>2.3.CO;2](https://doi.org/10.1130/0091-7613(1998)026<0127:ROGWIT>2.3.CO;2)